THE IDENTIFICATION AND CHARACTERIZATION OF NOVEL ANTIMICROBIAL PEPTIDES FROM THE ATLANTIC COD (*Gadus morhua*) GENOME

MITCHELL J. BROWNE

The identification and characterization of novel antimicrobial peptides from the Atlantic cod (*Gadus morhua*) genome

Mitchell J. Browne (B.Sc. Hons)

February 17, 2011, Memorial University of Newfoundland

Submitted in partial fulfillment of the requirements for the degree Master of Science

Department of Biochemistry

Memorial University of Newfoundland

St. John's, NL A1B 3X9

2010

Abstract

Antimicrobial peptides (AMPs) are short peptides that exhibit broad-spectrum activity against a variety of microbes including bacteria, viruses, fungi and protozoa. Based on previously generated Atlantic cod (*Gadus morhua*) expressed sequence tags (ESTs), I identified sequences representing four novel AMP-like transcripts [a peptide with sequence similarity to lipopolysaccharide binding protein (LBP), a transcript with sequence similarity to the potato (*Solanum tuberosum*) AMP snakin-2, as well as two piscidin-like peptides. The two peptides with similarity to the piscidins, a family of small cationic AMPs from fish, were selected for further study. I obtained full-length cDNA sequences for two paralogous piscidin-like transcripts using bi-directional rapid amplification of cDNA ends (RACE). The Atlantic cod paralogues were termed gaduscidins (GAD-1 and GAD-2), derived from the genus name *Gadus*. Quantitative reverse transcription – polymerase chain reaction (QPCR) was used in transcript expression studies of GAD-1 and GAD-2. I examined the constitutive expression of these transcripts in several tissues from non-stressed juvenile cod. Transcript expression of GAD-1 and GAD-2 was also examined in immune tissues following intraperitoneal (IP) injection of formalin-killed atypical *Aeromonas salmonicidia* (ASAL), or phosphate-buffered saline (PBS injection control). Putative GAD-1 and GAD-2 mature peptides were chemically synthesized for structural characterization, first using circular dichroism (CD) spectroscopy, followed by solution nuclear magnetic resonance (NMR). In addition to structural characterization, functional characterization was also carried out to determine hemolytic and antimicrobial activity of GAD-1 and GAD-2. A hemolytic assay against Atlantic cod red blood cells (RBCs) was performed, as well as a minimal

inhibitory concentration (MIC) assay for both GAD-1 and GAD-2 with *Staphylococcus intermedius* and *Escherichia coil.*

Acknowledgements

I would first like to thank my supervisors, Dr. Valerie Booth and Dr. Matthew Rise for their guidance and support. I would also like to thank Charles Y. Feng, Donna Jackman, and Dr. Michael Hayley, who helped me greatly throughout my project. Similarly, I would like to thank Tiago S. Hori, Dr. Marlies Rise, Jennifer R. Hall (Ocean Sciences Centre, Memorial University, NL, Canada), and Dr. David Heeley, Craig Skinner, Marie Codner, (Biochemistry Department, Memorial University, NL, Canada) as well ask Dr. Stewart Johnson (Fisheries and Oceans Canada, Pacific Biological Station, Nanaimo, B.C. Canada) for their help. I am also grateful for the funding I received from the Natural Sciences and Engineering Research Council of Canada (NSERC) as well as funding obtained for this project from Canada Research Chairs to both supervisors. In addition, I would like to thank LGL ltd. for the scholarship I received (The LGL Limited Scholarship in Marine Science). The Atlantic Cod Genomics and Broodstock Development Project (CGP), [which is funded by Genome Atlantic, Genome Canada, and the Atlantic Canada Opportunities Agency (ACOA)], facilitated the use of RNA samples used in this study. I would also like to thank the Dr. Joe Brown Aquatic Research Building (JBARB; Ocean Sciences Centre, Memorial University) staff as well as Jennifer Kimball, Sophie Hubert, and Dr Sharen Bowman at The Atlantic Genome Centre (Halifax, NS) for their involvement in the creation of the CGP EST database.

Note: A major portion of this thesis (gene expression studies, sequence characterization, etc.) contributed to the Developmental and Comparative Immunology paper entitled "Characterization and expression studies of Gaduscidin-1 and Gaduscidin-2, paralogous antimicrobial peptide-like transcripts from Atlantic cod (Gadus morhua) [Browne et al., 2010 (in press)]."

Table of Contents

List of Figures

List of Supplemental Material

Supplemental Figure S1. Brain nodavirus RT-PCR results for fish used in the QPCR studies to determine if high nodavirus carrier state significantly influenced brain, spleen, or head kidney GAD-1 or GAD-2 transcript expression.

Supplemental Table S1. Identification of transcripts representing GAD-1 (A) and GAD-2 (B), which were obtained from the Atlantic Cod Genomics and Broodstock Development Project (CGP) Expressed Sequence Tag (EST) database.

Supplemental Table S2. Mean pixel intensities of nodavirus RT-PCR products from individual Atlantic cod brain samples involved in this study.

Supplemental Table S3. QPCR Relative Quantification (RQ) data for the constitutive expression study of GAD-1 (A) and GAD-2 (B), normalized to 18S ribosomal RNA.

Supplemental Table S4. QPCR Relative Quantification (RQ) data for GAD-1 (A) and GAD-2 (B) and analysis of impact of nodavirus carrier state on expression of these transcripts in the brain, normalized to 18S ribosomal RNA

Supplemental Table S5. QPCR Relative Quantification (RQ) data for the study determining effect of nodavirus carrier state on expression of GAD-1 and GAD-2 transcripts in non-stressed (0 h) immune tissues, normalized to 18S ribosomal RNA

Supplemental Table S6. QPCR Relative Quantification (RQ) data for the immune tissue (head kidney and spleen) study indicating GAD-1 and GAD-2 transcript expression at four time points after intraperitoneal injection of phosphate-buffered saline (PBS) or formalin-killed, atypical *A. salmonicidia* (ASAL), normalized to 18S ribosomal RNA.

List of Abbreviations

0 h	individual Atlantic cod that were euthanized and sampled prior to injection
1D	one-dimensional
2D	two-dimensional
3D	three-dimensional
ACNNV	Atlantic cod nervous necrosis virus
AMP	antimicrobial peptide
ASAL	formalin-killed atypical *Aeromonas salmonicidia*
BLAST	basic local alignment search tool
BSA	bovine serum albumin
CD	circular dichroism
cDNA	complimentary DNA
CGP	Atlantic cod genomics and broodstock development project
contig	contiguous sequence
DMF	dimethylformamide
DMPC	dimyristoylphosphatidylcholine

DMPG	dimyristoylphosphatidylglycerol
DPPC	dipalmitoylphosphatidylcholine
DSS	4,4-dimethyl-4-silapentane-1-sulfonic acid
EST	expressed sequence tag
Fmoc	O-fluorenylmethyloxycarbonyl
GAD	gaduscidin
GOI	gene of interest
GNNV	grouper nervous necrosis virus
hBD	human ß-defensin
HNP	human neutrophil peptide
HoBt	1-hydroxy-benzotriazole
HPI	hours post-injection
HPLC	high-pressure liquid chromatography
IL	interleukin
IFN	interferon
IP	intraperitoneal
JNK	c-Jun NH(2)-terminal kinase

LPS	lipopolysaccharide
MHB	Mueller-Hinton broth
MIC	minimal inhibitory concentration
NMR	nuclear magnetic resonance
NOESY	nuclear Overhauser effect spectroscopy
PBS	phosphate-buffered saline
PC	phosphatidylcholine
PE	phosphatidylethanolamine
PG	phosphatidylglycerol
POPC	1-palmitoyl-2-oleoyl-*sn*-glycero-3-phosphocholine
POPG	1-palmitoyl-2-oleoyl-*sn*-glycero-3-phospho-(1'-rac- glycerol)
QPCR	quantitative reverse transcription – polymerase chain reaction
RACE	rapid amplification of cDNA ends
RBC	red blood cell
RQ	relative quantity
rRNA	ribosomal RNA
RT-PCR	reverse transcription – polymerase chain reaction

SDS	sodium dodecyl sulfate
SSH	suppression subtractive hybridization
TFE	2,2,2-Trifluoroethanol
TOCSY	total correlation spectroscopy
TMS	tricaine methanesulphonate

1. Introduction

Antimicrobial peptides (AMPs) are often small (12-50 residue), cationic peptides that represent an important component of innate immunity in many organisms. AMPs can exhibit antimicrobial activity against bacteria, viruses, protozoa, as well as fungi (Zasloff et al., 2002), and some have also been shown to exhibit anti-tumor activity (Rege et al., 2007). Importantly, many AMPs can kill microbial and tumor cells at concentrations that have little effect on mammalian cells (Rege et al., 2007, Hoskin and Ramamoorthy 2008). In many cases, AMPs disrupt the membranes of target cells, causing leakage of cell contents. However, interactions with intracellular targets are also believed to be an important component of activity for some AMPs (Nicolas, 2009). In addition, the immunomodulatory properties of AMPs represent another important component of their activity in humans and other mammals (Mookherjee et al., 2007). For example, mammalian AMPs have been shown to influence chemotaxis, cytokine release, antigen presentation, receptor interaction, angiogenesis, and wound healing (Lai and Gallo, 2009). The potential of AMPs to act on pathogenic and tumor cells without harming normal host cells makes them attractive candidates for novel therapeutics.

Structurally, AMPs can be generally classified into three categories: i) peptides with a disulfide bonded ß strand or α-helix (e.g. defensins), ii) α-helical peptides such as insect cecropins, amphibian magainins, or fish piscidins, and iii) peptides with an over-representation of a particular amino acid (Pro, His, Gly, Trp) which may fit into either structural category. ß-strand peptides such as protegrin-1, which are disulphide-bond stabilized, have well-defined structures in aqueous solution (Khandelia et al., 2008). However, the α-helical AMPs are often in an unstructured random-coil configuration in

aqueous solution, but adopt α-helical conformation in the presence of lipid membranes. Taking on this conformation allows the AMPs to interact with each other, and with the lipids, disrupting the bilayer.

There are generally four proposed mechanisms for membrane disruption: i.) the barrel-stave mechanism (Figure 1A; Baumann et al., 1974), ii.) the carpet mechanism (Figure 1B; Pouny et al., 1992), iii.) the toroidal pore mechanism (Figure 1C; Ludtke et al., 1996) and iv.) the disordered toroidal pore mechanism (Figure 1D; Leontiadou et al., 2006). In order for AMPs to disrupt membranes by any of these mechanisms, a threshold concentration of AMPs at the bilayer surface is required (Melo et al., 2009). Baumann et al (1974) first introduced the barrel-stave model as a probable mechanism for ion channel formation by alamethicin from the fungi *Trichoderma viride*. This mechanism involves the hydrophobic portion of the α-helix interacting with the lumen of the bilayer (Palffy et al., 2009). Barrel-stave pore formation (Figure 1A) requires that the AMP spans the entire length of the membrane and, thus, AMPs that function by this mechanism are typically α-helical peptides of 20 residues or more (Rozek et al., 2000). There are many examples of AMPs that fit this size criterion, and are believed to disrupt membranes in a similar manner to the barrel-stave mechanism. Examples include the 31-residue mammalian cecropin p1 (Gazit et al., 1996), the 20-residue fungi AMP alamethicin (Tieleman et al., 1999), and the 15-residue gramicidin from *Bacillus brevis* (Arseniev et al., 1985).

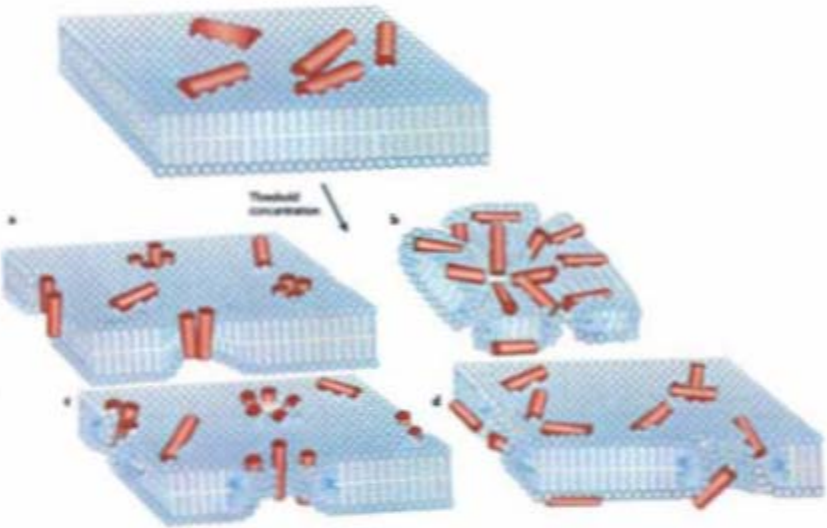

Figure 1. Four mechanisms by which AMPs may induce pore formation in a lipid membrane once threshold concentration is reached. Depiction of a) barrel-stave mechanism (Baumann et al., 1974) b) carpet mechanism, (Pouny et al., 1992), c) toroidal pore mechanism (Ludtke et al., 1996) and d) disordered toroidal pore mechanism (Leontiadou et al., 2006). Reprinted by permission from Macmillan Publishers Ltd: [Nature Reviews: Microbiology] (Melo et al., 2009), copyright (2009).

Some AMPs such as the aurein AMPs from frog (*Xenopus laevis*), with 13-17 amino acid residues in length, are not long enough to conform to the barrel-stave mechanism (Rozek et al., 2000). Many of these shorter peptides are thought to disrupt membranes via the carpet mechanism. This mechanism (Figure 1B) is described best by the AMP forming a 'carpet' on the membrane surface, which acts like a detergent, and induces pore-formation by the removal of micelle-like structures from the bilayer (Palffy et al., 2009). AMPs that disrupt membranes by this mechanism include the 26-residue bee venom AMP melittin (Smith et al., 1994), 22-residue frog magainin (Ludke et al., 1995), and frog dermaseptin b (Strahilevitz et al., 1994). Toroidal pore formation (Figure 1C) is similar to the barrel-stave mechanism, but in the case of the former, the AMP is always associated with the lipid head-groups. This association induces a connection between inner and outer membrane leaflets (Palffy et al., 2009) and, thus, the pore is lined with both lipid head-groups and peptides (Yang et al., 2001).

These mechanisms for membrane disruption have been derived from a variety of biophysical studies, in particular nuclear magnetic resonance (NMR). For example, using solid-state NMR, Tang et al (2009) determined that the cationic beta-hairpin AMP PG-1 induced torroidial pore-like changes in an anionic dilauroylphosphatidylcholine (DLPC) membrane mimetic. In addition, they showed that varying the number of cationic residues changes the orientation of the AMP in the membrane mimetic, as well as the level of insertion (Tang et al., 2009). Leontiadou et al (2006) introduced the disordered pore mechanism (Figure 1D) as a possible mechanism for pore formation in a dipalmitoylphosphatidylcholine (DPPC) bilayer by magainin MG-H2, an analogue of frog magainin. This mechanism differs from the traditional toroidal-pore mechanism in

that only one peptide is found at the centre of the pore while all others peptides are found on the edge of the pore, parallel to the bilayer surface.

In addition to the four generally accepted mechanisms discussed above, it has also been suggested that the segregation of components of the bacterial membrane into domains. Domain formation increases permeability, and, thus, is a possible mechanism of disruption of the bacterial membrane; Epand *et al* (2009) demonstrated domain formation in a (75:25) 1-palmitoyl- 2-oleoyl phosphatidylethanolamine (POPE) and tetraoleoyl cardiolipin (TOCL) model membrane upon addition of C12K–7-α-8, a highly cationic AMP using differential scanning calorimetry.

While the mechanism of membrane disruption is an important consideration, it is only one parameter in understanding the complex means of AMP-induced cell death. Another important aspect of AMPs function is their specificity for pathogen membranes in comparison to host cell membranes. This is thought to derive primarily from the difference in lipid composition and, thus, physicochemical characteristics (anionic, zwitterionic, cationic) of the lipids in the host versus microbial membrane. Bacterial membranes are commonly composed of the phospholipids cardiolipin (CL), phosphatidylglycerol (PG), and phosphatidylethanolamine (PE) (Epand et al., 2009), as well as peptidoglycan. However, Gram-negative species also contain lipopolysaccharides and lipoproteins, and Gram-positive species also contain teichoic acids and lipoids. In addition, both bacterial Gram-negative and Gram-positive cells have high variability in their membrane composition. For example, the Gram-positive species *Staphylococcus aureus* has approximately 80% PE in its membrane, while *Bacillis polymyxa*, also Gram-positive, has 0% PE (Epand et al., 2009). There is also variability in CL and PG content

between Gram-positive and Gram-negative bacterial species. In general, studies of AMP-membrane interactions are limited to phospholipid membrane mimetics. While such studies with simplified lipid systems have been valuable in suggesting models for the mechanisms of AMP membrane disruption and specificity, the interactions can be expected to be much more complex *in vivo*.

Interactions between AMP and membranes are important in the study of AMPs, as they often induce cell death by membrane disruption. However, interactions with microbial intracellular targets are also believed to be an important component of activity for some AMPs. For example, AMPs have been shown to inhibit DNA and protein synthesis, cell wall and cytoplasmic membrane synthesis, chaperone-assisted protein folding, enzyme activity (Nicolas, 2009), as well as energy dissipation through mitochondrial interaction (Westerhoff et al., 1989). AMPs such as the insect pyrrhocoricin and drosocin are believed to enter microbial cells through a receptor interaction, and once inside, interfere with either the chaperone DnaK, or inhibit DNA or protein synthesis (Kragol et al., 2002; Otvos et al., 2005). Human histatin-5, a histidine-rich AMP, is transported across the membrane in the protozoa *Leishmania* in a non-perturbing manner, where it causes energetic failure of the cell by accumulating in the mitochondrion, and inhibiting ATP synthesis (Luque-Ortega et al., 2008). Cell death by AMP-induced energetic collapse has also been reported in *Candida albicans* (Helmerhorst et al., 1999). Patrzykat et al (2002) determined that P-der, a hybrid between winter flounder (*Pseudopleuronectes americanus*) pleurocidin and frog dermaseptin, inhibits intracellular functions without damaging the *E. coli* cytoplasmic membrane: P-der inhibited microbial RNA synthesis, but further studies are required to determine if

this is the primary target (Patrzykat et al., 2002). Despite all of the AMPs that have been recently described (over 1,600 in the AMP Database, http://aps.unmc.edu/AP/main.php), relatively few AMPs have been conclusively proven to enter microbial cells and affect processes within.

Membrane disruption, and interactions with intracellular targets are two important means of AMP-induced microbial death. In addition, many AMPs aid host microbial clearance with immunomodulatory properties and, thus, influence immune cell migration and proliferation, as well as the expression of immune mediators (Easton et al., 2009). For example, the human cathelicidin hCAP18/LL-37 induces chemokine production, and acts as a chemoattractant for mast cells (Niyonsaba et al., 2001), dendritic cells (Davidson et al., 2004), neutrophils (Zheng et al., 2007), and monocytes (Mookherjee et al., 2006). LL-37 also induces mast cell de-granulation (Niyonsaba et al., 2001), and can effectively inhibit apoptosis of neutrophils *in vitro* (Barlow et al., 2006). Similarly, the α-defensins human neutrophil peptides (HNP) 1 and 2 are chemotactic for monocytes (Territo et al., 1989), and the human ß-defensins (hBD) 3 and 4 are chemotactic for monocytes and macrophages (Yang et al., 2002). In addition, human α and ß defensins are chemotactic for memory T cells (Lai and Gallo, 2009), representing a link between the innate and adaptive immune systems. Defensins and cathelicidins, which are produced by epithelial cells and keratinocytes, provide a vital innate immune role against microbial invasion at these sites (Yang et al., 2001). For example, Van Wetering et al (1997) determined that HNP stimulates interleukin (IL)-8 production in human airway epithelia; IL-8, in turn, is a neutrophil chemoattractant, further enhancing the immune response.

In order to properly understand the immunomodulatory properties that AMPs possess, signaling pathways that control immune regulation must first be understood. Although there have been few studies of signaling pathway regulation of AMPs in fish, much is known about regulation of signaling pathways by human and insect AMPs. Regulation of expression of human AMPs is mediated by pathogen-associated molecular pattern (PAMP) receptors (e.g. Toll-like receptors (TLR) or release of cytokines (Lai and Gallo, 2009). The human ß-defensins hBD2-4 are induced by stimulation of TLR ligands, IL-1ß, interferon (IFN)-γ, and tumor necrosis factor (Selsted et al., 2005), whereas cathelicidin is regulated by histone deacetylation (Kida et al., 2006) and the vitamin D receptor (Wang et al., 2004). The signaling pathways regulating expression of AMPs in humans are further complicated by their major integration with the adaptive immune system.

Insects, however, lack an adaptive immune system, and, thus, rely heavily on their innate immunity. Their response to invading pathogens is to rapidly produce AMPs and release them into circulation (Aggarwal et al., 2008). The release of an array of AMPs is induced by nuclear factor κ-light-chain-enhancer of activated B cells (NF-κB)-like transcription factors, which are governed by the Toll, Janus kinase-signal transducer and activator of transcription (JAK-STAT), c-Jun NH(2)-terminal kinase (JNK), and immune deficiency (IMD) pathways. Much is known about the pathways regulating the innate immune response in *Drosophila*; however, interactions between these pathways are not fully understood. Furthermore, pathway regulation by non-immune interactions is also present. For example, Radyuk et al (2010) demonstrated that peroxiredoxin-5, a redox enzyme, acts as a regulator of the immune response in *Drosophila melanogaster* by

modulating the JNK pathway, which results in greater resistance to bacterial infections. Even though AMP studies in fish have thus far largely not included analysis of signaling pathways, it has been suggested that Atlantic cod cathelicidin up-regulation may be associated with the TLR-9 signaling cascade (Feng et al., 2009). Similarly, Feng et al (2009) determined that bacterial stimulation induced, along with transcripts encoding the putative AMPs cathelicidin and hepcidin, other immune-relevant transcripts such as IL-1ß, IL-8, and IFN regulatory factor-1 (IRF1). It is possible that fish AMPs may share similarity in regulation with human and insect examples. In addition, fish AMPs may play a role in linking the innate and adaptive immune system, a hypothesis that requires further investigation.

Mining of naturally occurring AMP sequences for novel motifs of potential use in human medicine via genomic and proteomic approaches provides access to the hundreds of millions of years of molecular evolution that contributed to the catalogue of AMPs used by extant organisms. Peptide therapeutics based on natural AMP sequences have the potential to reduce the reliance of modern medicine on traditional antimicrobial therapeutics, an important concern given the increasing problem of antibiotic resistance. The lack of structurally novel antibiotics in recent decades (Spellberg et al., 2004) combined with the emergence of "superbugs" such as methicillin-resistant *Staphylococcus aureus,* have resulted in a great need for novel therapeutics.

Marine organisms represent a potentially fruitful resource for novel antimicrobial discovery as these organisms rely heavily on their innate immune systems to combat the constant threat of infection in the marine environment (Patrzykat and Douglas 2003). Fish AMPs have been previously shown to exhibit microbial killing potency 12-100

times that of amphibian AMPs against numerous pathogens (Park et al., 1998). Administration of pleurocidin-amide (a 25-residue, C-terminally amidated AMP) into the peritoneal cavity of coho salmon (*Oncorhynchus kisutch)* using a miniosmotic pump significantly reduced mortality from 67-75% in the control (no AMP administration) group to 5% following intraperitoneal (IP) challenge of *Vibrio anguillarum* (Jia et al., 2000). This study demonstrated the ability of a fish AMP to protect the host against pathogenic bacteria *in vivo* (Jia et al., 2000), which suggests that new strategies may be developed for using AMPs to prevent bacterial diseases of fish.

Over 1,600 low molecular weight, cationic AMPs have been identified from various organisms (The AMP Database, http://aps.unmc.edu/AP/main.php) including fish. The piscidins are a family of AMPs common to many fish species. These peptides have widespread distribution in fish (Silphaduang et al., 2006), and share the properties of an α-helical structure, low molecular weight, broad-spectrum antimicrobial activity, and cationic charge at physiological pH. The piscidin family includes AMPs such as pleurocidin moronecidin, chrysophsin, dicentracin, epinecidin, and myxinidin (Cole et al., 1997; Lauth et al., 2002; Iijima et al., 2003; Salerno et al., 2007; Pan et al., 2007; Subramanian et al., 2009).

Many studies of AMP expression patterns, including this one, make use of mRNA analysis. AMP-coding genes in fish are expressed at the mRNA level in a broad range of tissues. Pleurocidin mRNA was first detected in winter flounder skin (Cole et al., 2000), and as well as in intestinal epithelia (Cole et al., 1997; Douglas et al., 2003). Moronecidin gene expression in hybrid striped bass (a hybrid generated from *Morone saxatilis* and *Morone chrysops*) was detected by quantitative reverse transcription - polymerase chain

reaction (QPCR) in gill, skin, intestine, spleen, head kidney, and blood (Lauth et al., 2002). Another fish AMP derived from grouper (*Epinephelus coioides*) epinecidin-1, had transcripts in head kidney, intestine, and skin as detected by RT-PCR (Pan et al., 2007). Mandarin fish (*Siniperca chuastsi*) piscidin mRNA was determined by QPCR to be located in intestine, head kidney, and spleen (Sun et al., 2007). Recently, expression of AMP-coding transcripts was discovered in a number of fish immune-relevant cells. Transcript expression of dicentracin from sea bass (*Dicentrarchus labrax*) was observed in peripheral blood, kidney and peritoneal cavity leukocytes by *in situ* hybridization (Salerno et al., 2007). Similarly, dicentracin mRNA was detected in sea bass granulocytes and monocytes in blood and kidney, as well as in peritoneal cavity-derived macrophages using *in situ* hybridization (Salerno et al., 2007).

Bacterial challenge is a useful means of assessing expression patterns of AMPs. It is known that some fish AMP transcripts are inducible by attenuated bacteria or PAMP [e.g. lipopolysaccharide (LPS)] challenge, while others do not respond significantly to bacterial antigens. Using QPCR, Feng *et al.* (2009) showed that both cathelicidin and hepcidin transcripts were significantly up-regulated by formalin-killed atypical *Aeromonas salmonicidia* (ASAL) in Atlantic cod spleen and head kidney. Using QPCR, Sun *et al.* (2007) showed that moronecidin transcripts from Chinese perch were up-regulated by LPS in brain, gill, kidney, head kidney, skin, intestine, and spleen. However, a QPCR study of the effect of *Streptococcus iniae* challenge on moronecidin transcript expression in hybrid striped bass indicated that the bacterial challenge did not result in up-regulation (greater than four-fold higher as compared to mock-injected) of moronecidin in blood, gill, head kidney, intestine, liver, or skin, (Lauth et al., 2002).

With this project, I set out to identify and characterize novel AMPs from the Atlantic cod transcriptome for use in future human medicine. The identification process used bioinformatic techniques including hidden-Markov model-based software to identify AMP-like motifs from translated expressed sequence tag (EST) sequences obtained from the Atlantic Cod Genomics and Broodstock Development Project (CGP, http://codgene.ca) database. Once antimicrobial motifs were found, the putative AMP-coding transcripts were sequenced, and the correct open reading frame (ORF) was deduced to determine the putative mature AMP sequence. Also, constitutive expression of these AMP-coding transcripts was assessed in a number of tissues (head kidney, blood, brain, gill, pyloric caecum, and spleen), as well as in head kidney and spleen upon bacterial antigen challenge. In addition, impact of nodavirus carrier state on gaduscidin transcript expression in head kidney and spleen was assessed. Next, the putative mature AMPs were chemically synthesized, assessed structurally using CD and NMR, and subjected to functional antimicrobial assays against a Gram-positive and Gram-negative species. Finally, hemolytic assays were performed to determine any hemolytic effects against eukaryotic erythrocytes.

2. Materials and methods

2.1. QPCR sample preparation: tissue collection and bacterial antigen preparation and stimulation

QPCR sample preparation started with collecting tissues from juvenile Atlantic cod that had been stimulated with a saline injection control or bacterial antigens. The fish used in this study were from a single family (Family 32, CGP 2006 year class). The cod (~25 g each) were reared in 500-litre tanks maintained with flowing seawater (10°C, 90% O_2 saturation) and kept on a 12 h light 12 h dark photoperiod. Fish were fed daily at 1.5 % body mass/day for 17 days and kept in separate tanks for two groups: 1) a control group that was given an intraperitoneal (IP) injection with 100 µl of phosphate-buffered saline (PBS), and 2) an experimental group that was IP injected with 100 µl of formalin-killed atypical *Aeromonas salmonicidia* (ASAL tank). Immediately prior to stimulation, fish were injected with a lethal dose of 0.4 g/l of tricaine methanesulphonate (TMS) (Syndel Laboratiries Vancouver, BC, Canada). Tissues used in the study were excised, flash-frozen in liquid nitrogen, and stored at -80°C until RNA extraction. For the ASAL and PBS groups, the hematopoietic kidney (anterior or head kidney) and spleen tissues (Figure 2) were collected from eight individuals prior to injection (0 h), and at 2, 6, 24, and 72 h post-injection (HPI) (Feng et al., 2009). Constitutive GAD-1 and GAD-2 transcript expression was also examined in blood, brain, gill, head kidney, pyloric caecum and spleen (Figure 2) of 6 non-stressed (0 h) cod. All tissue samples were flash-frozen in liquid nitrogen, and RNA samples were DNase I-treated and column-purified as previously described (Feng et al., 2009; Rise et al., 2008). It should be noted that Rise lab

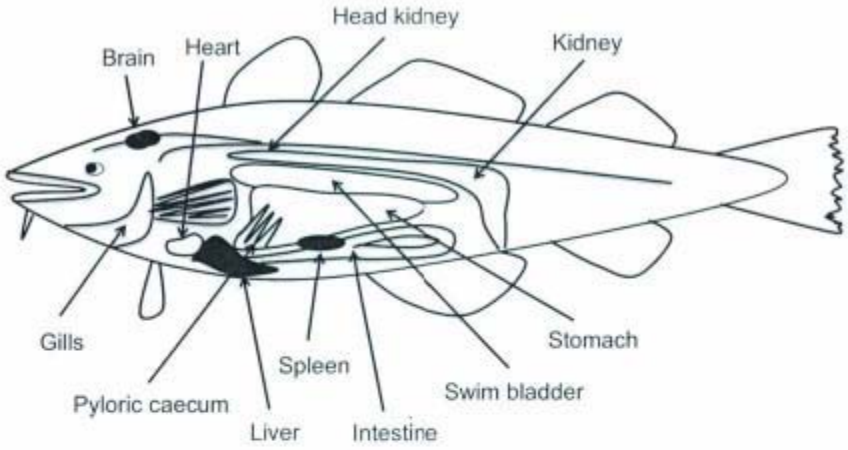

Figure 2. A depiction of Atlantic cod (*Gadus morhua*) internal anatomy, including tissues sampled for this study.

members carried out the cod rearing, stimulation, and sampling work prior to my arrival in the lab; however, as part of my honours research, I did RNA extractions from numerous tissues used in this study.

2.2. Identification of transcripts encoding Atlantic cod putative AMPs

The CGP EST database was first probed for sequences containing AMP motifs using AMPer, a hidden Markov model-based software (Fjell et al., 2007). In addition, the EST database was searched for sequences with antimicrobial annotation as determined by AutoFACT (Koski et al., 2005). A contiguous sequence (contig all_v2.0.10048.C1) with antimicrobial annotation was found, and hypothetical translations of this transcript were probed for AMP-like motifs, also using AMPer. Further analysis revealed that the contig contained four ESTs (GenBank accession numbers FG315061, EY972641, EY973733, and EY974225) (Table 1, Supplemental Table S1), and encoded a putative AMP. Based on tBLASTn alignment of the contig all_v2.0.10048.C1 sequence against the CGP EST database Bowman et al. 2010 (in press), I identified a contig containing two ESTs (all_v2.0.3805.C2; accession numbers FF411786 and ES773100) (Table 1, Supplemental Table S1) representing a second, related cod AMP-like transcript.

2.3. Determination of full-length cDNA sequences for Atlantic cod GAD-1 and GAD-2

The full-length cDNA sequences of GAD-1 and GAD-2 were obtained using RNA ligase-mediated (RLM) rapid amplification of cDNA ends (RACE). Full-length

Table 1. Identification of gadusicidin transcripts in the CGP database.

Gene	Library type[1]	CGP library identifier[2]	Tissue	Treatment[3]	No. of clones[4]
GAD-1	SSH forward	gmsllkfas	head kidney	ASAL	1
	SSH reverse	gmsllkras	head kidney	ASAL	2
	Normalized	gmllhgnts	gill	none	1
GAD-2	SSH forward	gmsllsflc	spleen	pIC	4
	Normalized	gmsllhkxw	head kidney	ASAL	1
	Normalized	gmsllZpis	blood	ASAL& pIC	1
	SSH forward	gmsllcfta	head kidney	heat shock	1

[1]The forward SSH libraries were constructed to be enriched for transcripts up-regulated by the treatment (ASAL, pIC, or thermal stress). Reverse SSH libraries were constructed to be enriched for transcripts down regulated by the treatment (ASAL, pIC, or thermal stress). Normalized cDNA libraries were constructed to normalize the abundance of transcripts in order to maximize gene discovery (Bowman et al., 2010).

[2]The identifiers (i.e. names) of the SSH libraries in the CGP EST database (http://codgene.ca) are provided Bowman et al. (in press).

[3]The ASAL (bacterial antigen), pIC (viral mimic), and the heat stress stimulation procedures were described previously (Feng et al. 2009; Rise et al. 2008; and Hori et al. 2010).

[4]The number of clones does not necessarily equate to the number of ESTs (listed in Table S1), as some clones were sequenced more than once. A complete listing of all ESTs with accession numbers can be found in Supplementary Table S1.

RACE-ready cDNA was synthesized using the GeneRacer Kit (Invitrogen, Burlington, ON). Briefly, 250 ng of spleen poly(A)$^+$ RNA (mRNA) was isolated from a pool of total RNA from 20 ASAL-stimulated juvenile cod as previously described (Feng et al., 2009). Based on assembled ESTs (see section 2.2), gene-specific primers (Table 2) for GAD-1 and GAD-2 were designed using the Primer3 program (Rozen and Skaletsky, 2000, http://frodo.wi.mit.edu). RACE used a touch-down PCR followed by a nested PCR as specified in the GeneRacer Kit manual, with an extension time of 3 min for all cycles. For both 5' and 3' RACE, PCR using 1 µl of RACE cDNA (250 ng of input RNA) as template was followed by nested PCR. For both PCR reactions, the GeneRacer 5' and 3' primers as well as the GAD-1 and GAD-2 gene specific primers were used (Figure 3 and Table 2). Cycling parameters for 5' and 3' RACE consisted of an initial denaturation period of 2 min at 94°C, followed by 25 cycles of (94°C for 30 sec, 70°C for 30 sec, 72°C for 3 min), and 1 cycle at 68°C for 10 min. For 5' and 3' nested RACE, cycling parameters consisted of 2 min at 94°C, followed by 25 cycles of (94°C for 30 sec, 65°C for 30 sec, 68°C for 2 min), and 1 cycle at 68°C for 10 min. GAD-1 and GAD-2 sequences were amplified using the Advantage 2 Polymerase Kit (Clontech, Mountain View, CA) following the manufacturer's instructions. PCR products were extracted from a 1% agarose gel (made with 1X TAE buffer, and stained with ethidium bromide) using the QIAQuick Gel Extraction Kit (QIAGEN, Mississauga, ON) following the manufacturer's instructions. Upon washing, ethanol precipitation, and resuspension in nuclease-free water (Invitrogen), gel-extracted PCR products were cloned into the pCR2.1-TOPO vector (Invitrogen) following the manufacturer's instructions. Recombinant vectors were transformed into TOP10 chemically competent *E. coli* cells

Table 2. Primers used for QPCR gene expression analysis and bi-directional RACE in this study.

Primer name[1]	Oligonucleotide sequence (5'-3')	Application[2]
Nodavirus AC2F1	GTGGTTACGTGGCTGGCTTC	Nodavirus diagnostic RTPCR
Nodavirus AC2R4	GTTCTGCTTTCCCACCATTTG	
GAD1-*f*	AGTCCTCCACCAACAGCATC	QPCR (87%, 101 bp)
GAD1-*r*	TGAAACATGCGAACTGCAAG	
GAD2-*f*	TCAAAAGGTTCCAGTTTCCAG	QPCR (87%, 151 bp)
GAD2-*r*	GTGGATCAAACCCACGATGT	
18S-*f*	ATGGCCGTTCTTAGTTGGTG	QPCR Normalizer (95%, 180 bp)
18S-*r*	GGACATTTAAGGGCGTCTCA	
GAD1-f3	CGTGCTGCTTCTGGCCATGATGGTT	3'RACE
GAD1-r1	CAGCTTTTTCTCCATGGATGGCACGAT	5'RACE
GAD1-f2	TCCATCACATCATCGGGTGGATCAGC	3' Nested RACE
GAD1-r2	ATGGCCCTCACACACCATGGCTGATCC	5' Nested RACE
GAD2-f3	GTGCTGCTTCTGGCCATGATGGTTCTG	3'RACE
GAD2-r1	CTCTGTTCGAGTGTTCGCCGCTGCTGT	5'RACE
GAD2-f2	AGCTGGAGGCTTTTTGCACCACATCGT	3' Nested RACE
GAD2-r2	TGCACGGTCACCGAAGAGAGACAAACC	5' Nested RACE
GeneRacer 3' Primer	GCTGTCAACGATACGCTACGTAACG	3'RACE
GeneRacer 5' Primer	CGACTGGAGCACGAGGACACTGA	5'RACE
GeneRacer 3' Nested Primer	CGCTACGTAACGGCATGACAGTG	3' Nested RACE
GeneRacer 5' Nested Primer	GGACACTGACATGGACTGAAGGAGTA	5' Nested RACE

[1] "f" or "r" refers to forward or reverse primer orientation and is preceded by the gene name.

[2] Amplification efficiency calculations for QPCR primers can be found in the Materials and methods (section 2.6).

GAD-1


1 ATCTCTACCTGTCGAAAGGTT 21
22 CCAGTTTACAGCTTCAAATCAGAGCTCAAATCGGTATCTGAAAGG 66
67 ATGAGGTATATTGTTCTACTTGTTGTCGTGCTGCTTCTGGCCATG 111
M R Y I V L L V V V L L L A M
112 ATGGTTCAGCCAGCAGACTGCTTTATCCATCACATCATCGGGTGG 156
M V Q P A D C F I H H I I G W
157 ATCAGCCATGGTGTGAGGGCCATCCATCGTGCCATCCATGGAGAA 201
I S H G V R A I H R A I H G E
202 AAAGCTGAGGAATATATTATGGTGGATTAGTCCTCCACCAACAGC 246
K A E E Y I M V D .
247 ATCGGCAAACACTCGAACAGAGCCGTTGTTGCACATGCCGAACAA 291
292 GAAGAACAAGCATGCTAACCTTGCAGTTCGCATGTTTCAAGTTTT 336
337 AATGTAAATGGCATGTTGGTGATAAATAAATAGGCATTATAAACA 381
382 TAAAAAAAAAAAAAAAAAAAAAAA 405
F1
F2
R2
R1
F
R

GAD-2

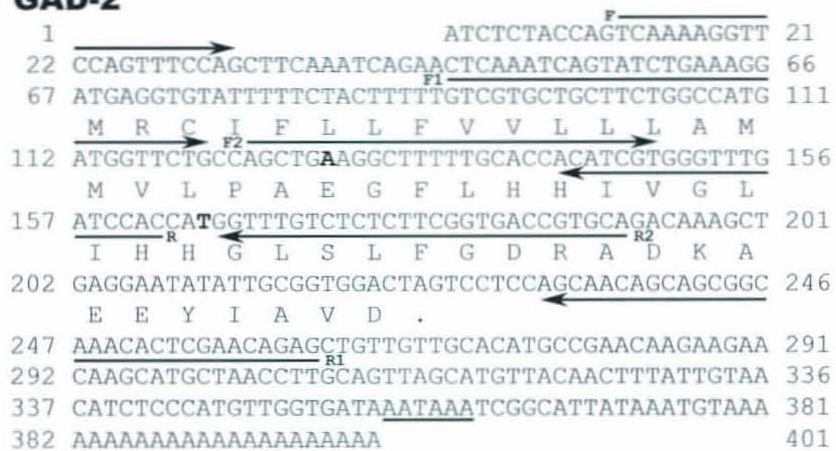
1 ATCTCTACCAGTCAAAAGGTT 21
22 CCAGTTTCCAGCTTCAAATCAGAACTCAAATCAGTATCTGAAAGG 66
67 ATGAGGTGTATTTTTCTACTTTTTGTCGTGCTGCTTCTGGCCATG 111
M R C I F L L F V V L L L A M
112 ATGGTTCTGCCAGCTGAAGGCTTTTTGCACCACATCGTGGGTTTG 156
M V L P A E G F L H H I V G L
157 ATCCACCATTGGTTTGTCTCTCTTCGGTGACCGTGCAGACAAAGCT 201
I H H G L S L F G D R A D K A
202 GAGGAATATATTGCGGTGGACTAGTCCTCCAGCAACAGCAGCGGC 246
E E Y I A V D .
247 AAACACTCGAACAGAGCTGTTGTTGCACATGCCGAACAAGAAGAA 291
292 CAAGCATGCTAACCTTGCAGTTAGCATGTTACAACTTTATTGTAA 336
337 CATCTCCCATGTTGGTGATAAATAAATCGGCATTATAAATGTAAA 381
382 AAAAAAAAAAAAAAAAAAAA 401
F
F1
R
R2
R1

Figure 3. The full-length cDNA sequences with putative translations for GAD-1 (A), and GAD-2 (B). Gene specific primers that were used for cloning (see Table 2 and Section 2.3) are denoted as arrows (forward primers: arrows above the nucleotide sequence; the reverse primers: arrows below the sequence). The translation is shown below the putative open reading frame (ORF), with the stop codon shown as a period. The AATAAA polyadenylation signal is underlined. In the GAD-2 sequence, the single nucleotide polymorphisms (SNPs) at positions 128 (A-G) and 165 (T-C) are shown in bold font.

(Invitrogen), and cells were grown for 16 hours at 37°C on LB/agar/ampicillin (50 µg/ml) plates containing bromo-chloro-indolyl-galactopyranoside (1.6 mg/plate) for blue/white colony selection. Individual colonies were cultured at 37°C for 16 hours in LB/carbenicillin (50 µg/ml). Plasmid DNA samples were prepared and isolated in the 96-well format using standard methods. Prior to sequencing, recombinant plasmid insert sizes were determined by *Eco*RI (Invitrogen) digestion and visual assessment of the restriction fragments on a 1% agarose gel run with the 1 Kb Plus ladder (Invitrogen). In order to give at least 6-fold coverage for the GAD-1 and GAD-2 sequences (i.e. to ensure high quality consensus sequences), at least 3 individual clones were sequenced twice in both directions using the ABI 3730 DNA Analyzer with BigDye Terminator chemistry (Applied Biosystems, Foster City, CA). Sequencing was performed at the Genomics and Proteomics Facility (GaP), Memorial University.

2.4. Effect of nodavirus carrier state on GAD-1 and GAD-2 transcript expression

Nodavirus RT-PCR testing was conducted by Charles Y. Feng (Ocean Sciences Centre, Memorial University) on a set of unstressed (0 h pre-injected) individuals that had previously been shown to include some asymptomatic nodavirus carriers (Rise et al. 2008; Feng et al., 2009; Rise et al., 2010). For each individual involved in the study, 1 µg of DNAse-I treated, column-purified brain total RNA was reverse transcribed using Moloney murine leukemia virus (M-MLV) reverse transcriptase and random hexamers (Invitrogen) at 37°C for 50 min in a final reaction volume of 20 µl as in Rise et al. (2008). The resulting cDNA was diluted with nuclease-free water (Invitrogen) to a final

volume of 200 µl. The PCR amplification was performed using DyNAzyme EXT DNA polymerase (MJ Research,Waltham, MA). Each PCR reaction contained 1 U of DyNAzyme EXT DNA polymerase, 1X manufacturer's optimized DyNAzyme EXT Buffer, 0.2 mM dNTPs, 4 µl of diluted cDNA (20 ng of input total RNA), and 0.2 µM each of nodavirus specific primers AC2F1 and AC2R4 (Table 2). PCR cycling conditions consisted of 40 cycles of (94°C for 30 sec, 61°C for 30 sec and 72°C for 10 sec). For each 50 µl PCR reaction, 5.5 µl of 10X Blue Juice (Invitrogen) was added and 15 µl of this mixture was electrophoretically separated on a 1.5 % agarose gel (stained with ethidium bromide and visualized under UV light) using a 100 bp ladder (Invitrogen) as a size marker. The area used for pixel intensity quantification was constant in each gel lane. Based on agarose gel images and pixel intensity data, individuals with no apparent visible nodavirus RT-PCR band (mean pixel intensity in the range 662 to 5887) were assigned to the "no/low" nodavirus carrier state and individuals with visible nodavirus RT-PCR bands (mean pixel intensity in the range 10,973 to 33,733) were assigned to the "high" nodavirus carrier state (Supplemental Figure S1 and Supplemental Table S2).

2.5. GAD-1 and GAD-2 putative open reading frame (ORF) sequence analysis

Based on the full-length cDNA sequences of GAD-1 and GAD-2, their respective open reading frames (ORFs) were deduced using BLASTx alignments and the Sequence Builder function of the Lasergene 7.20 software package (DNASTAR, Madison, WI). The MegAlign ClustalW function (Lasergene 7.20) was used to construct an amino acid sequence alignment of translated GAD-1, GAD-2 and their best Universal Protein Resource (UniProt; http://www.uniprot.org/) BLASTP hits (i.e. E-value $\leq$ 1). This

threshold was used because these two putative cod AMPs and other fish AMP-like sequences are relatively short (i.e. less than 90 amino acid residues), and poorly conserved. An unrooted phylogenetic tree was generated from this set of amino acid sequences using the MEGA 4 software (Tamura et al., 2007) and a ClustalX (Version 2.09) sequence alignment. The tree, constructed using the neighbor-joining method, was bootstrapped 10,000 times.

2.6. Quantitative reverse transcription - polymerase chain reaction (QPCR)

RNA extraction and purification were carried out as in Feng et al. (2009). QPCR was used to study: 1) constitutive GAD-1 and GAD-2 mRNA expression, 2) GAD-1 and GAD-2 transcript expression response to immune stimulation, and 3) the potential impact of high nodavirus carrier state (assessed by brain RT-PCR with nodavirus-specific primers, see section 2.4) on GAD-1 and GAD-2 transcript expression. The constitutive expression of GAD-1 and GAD-2 transcripts was determined in 6 tissues (head kidney, blood, brain, gill, pyloric caecum, and spleen) with 6 non-stressed (0 h pre-injected) juvenile cod (biological replicates) to assess biological variability. In the second QPCR study, the transcript expression response of GAD-1 and GAD-2 was analyzed in head kidney and spleen at four time-points (2, 6, 24, and 72 h) following IP injection with ASAL or phosphate buffered saline (PBS); for each time-point, seven biological replicates were used for each ASAL and PBS injection group. Pre-injected (0 h) control groups (n=7) were also included for each tank (i.e. ASAL tank and PBS tank). In the third QPCR study, the constitutive transcript expression of GAD-1 and GAD-2 in brain

was analyzed in individuals with high nodavirus carrier state (n=8) and individuals with no/low nodavirus carrier state (n=8). In addition, the effect of nodavirus carrier state on the transcript expression of GAD-1 and GAD-2 in head kidney and spleen was also analyzed by comparison of the constitutive transcript expression (i.e. the transcript expression in pre-injected individuals) in individuals with high nodavirus carrier state (n=5) and individuals with no/low nodavirus carrier state (n=7).

Primers for QPCR amplification of GAD-1 and GAD-2 (Table 2) were designed using the Primer3 program (Rozen and Skaletsky, 2000, http://frodo.wi.mit.edu). Primers for 18S rRNA (Table 2) amplification were the same as in Rise et al. (2008). For each QPCR primer pair (Table 2), a standard curve was generated to assess amplification efficiency, and a dissociation curve was generated to ensure that a single product was amplified. In addition, no-template controls were run to ensure that primer dimers were absent. Amplicons were also run on a 1.5% agarose gel with a 100 bp ladder (Invitrogen) to ensure amplicons were of the expected size. The amplification efficiency for the 18S rRNA primers (95%) differed from the previously determined efficiency for these primers (109% in Rise et al., 2008), possibly due to differences in samples and QPCR instruments used in the studies.

In all QPCR studies, the expression of GAD-1 and GAD-2 was normalized to the expression of 18S ribosomal RNA, which was stably expressed [threshold cycle (C_T) was within 1.5 cycles for all samples] in all samples. QPCR in the 96-well format was carried out with the Applied Biosystems 7500 FAST Real Time PCR system. For each sample, 1 µg of DNAse-I treated, column-purified total RNA was reverse transcribed using Moloney murine leukemia virus (M-MLV) reverse transcriptase and random hexamers

(Invitrogen) at 37°C for 50 min in a final reaction volume of 20 µl as previously described (Rise et al. 2008). The resulting cDNA was diluted with nuclease-free water (Invitrogen) to a final volume of 200 µl. The reaction volume for each QPCR amplification was 13 µl, and contained 2 µl of diluted cDNA (10 ng input total RNA), 1X Power SYBR green master mix (Applied Biosystems) and 50 nM of the forward and reverse primers (Table 2). The amplification protocol for the QPCR consisted of 1 cycle of 10 min at 95°C, followed by 40 cycles of (95°C for 15 sec, and 60°C for 1 min), with fluorescent signal measured at the end of each 60°C step. The transcripts of interest and normalizer amplifications were run in triplicate on the same plate for each sample. In addition, a control amplification reaction was run on every plate in each study to ensure that there was no technical variability among plate runs.

2.7. QPCR data collection and statistical analysis

The fluorescence thresholds and baselines were automatically set by the 7500 Fast Real-time PCR System software (Applied Biosystems 7500 fast v2.0). For technical replicates that were of low quality (indicated by 7500 Fast Real-time PCR System software flags), either the unacceptable technical replicate was removed (resulting in acceptable technical duplicates), or the triplicate reactions were repeated if dropping the outlier still resulted in a flag. In addition, the expression of the normalizer (18S) was used as an indicator to control for cDNA template quality. Samples with normalizer C_T deviating more than 0.75 cycles from the average C_T of all samples within the same study were removed from the analysis (see footnotes of Supplemental Tables S3 and S6). The

C_T values and amplification efficiencies (Table 2) for each gene of interest (GOI), and normalizer primer pairs were incorporated into the calculations of relative quantity (RQ) using the 7500 Fast Real-time PCR System software and the delta-delta C_T quantification method (Livak and Schmittgen, 2001).

All RQ values are presented as mean ± standard error (SE). For each QPCR study, the lowest normalized GOI, expression was set as the calibrator (i.e. RQ value of 1). For the constitutive expression study, a one-way analysis of variance (ANOVA) with Tukey post-tests was carried out on RQ values to determine if there was any statistical difference in basal transcript expression of GAD-1 and GAD-2 across the different tissues (head kidney, blood, brain, gill, pyloric caecum, and spleen). For the immune stimulation QPCR study, two-way ANOVAs were conducted on the RQ data obtained from head kidney and spleen for GAD-1 and GAD-2 to determine the effects of injection (i.e. ASAL or PBS) and time post-injection on GAD-1 and GAD-2 transcript expression. In addition, for both treatments, one-way ANOVAs with Tukey post-tests were conducted to determine if there were any effects of injection (PBS or ASAL) on GAD-1 and GAD-2 expression at 2, 6, 24, or 72 HPI as compared to the pre-injected (0 h) group, or if there was any difference in expression between the time-matched PBS and ASAL groups at each of the time points. To determine if high asymptomatic nodavirus carrier state had any effect on transcript expression in brain, head kidney, or spleen, two-sample t-tests were conducted on the GAD-1 and GAD-2 RQ values from individuals with either high nodavirus brains or no/low nodavirus brains (see Supplemental Figure S1 and Section 2.4). For all statistical assessments, Systat 12.0 (Systat Software Inc.) was used,

and data comparisons using t-tests, ANOVAs and Tukey post-tests were considered significant if $p \leq 0.05$.

2.8. Prediction of mature GAD-1 and GAD-2 peptide sequences

GAD-1 and GAD-2 full-length peptide sequences were input into the signalIP server (Nielsen et al., 1997; Bendtsen et al., 2004, http://www.cbs.dtu.dk/services/SignalP/) to predict if either contained a signal peptide motif. In addition, putative mature GAD-1 and GAD-2 sequences were predicted based on sequence similarity with known AMPs. Also, putative mature GAD-1 and GAD-2 sequences were also analyzed using a helical wheel model (University of California, Irvine Membrane Protein Explorer Version 3.2 helical wheel applet) to predict amphipathicity.

2.9. Peptide synthesis and purification

Putative mature GAD-1 (FIHHIIGWISHGVRAIHRAIH), and GAD-2 (FLHHIVGLIHHGLSLFGDR) were produced by solid-phase synthesis using O-fluorenylmethyloxycarbonyl (Fmoc) chemistry. For each peptide, Fmoc amino acids were weighed out in 5X excess and placed into a CS Bio peptide synthesizer (model CS336X, CS Bio Company Inc, Menlo Park, CA) using 0.43 g of a 0.47 mmol/g Rink amide resin (CS Bio Company Inc, Menlo Park, CA). Dissolution and de-blocking of amino acids were facilitated using a 0.4 M 1-hydroxy-benzotriazole (HoBt) dissolved in

dimethylformamide (DMF), and a 20% peperidine/DMF solution, respectively (Sigma-Aldrich Co., St. Louis MO). Resin washes were carried out with DMF. Upon completion of peptide synthesis, the resin containing synthesized GAD-1 or GAD-2 was transferred to a 10 ml syringe (BD Diagnostics Co.) equipped with a filter, and washed with methanol thoroughly under vacuum. The resin was then air dried for 30 min followed by vacuum desiccation for 60 min. Cleavage of the peptide from the resin was carried out using a solution of 9.4 ml trifluoroacetic acid (TFA), 0.25 ml 1,2-Ethanedithiol, 0.1 ml thioanisole (Sigma-Aldrich Co.), and 0.25 ml distilled water. The cleavage solution was added to the resin (3.5 ml) and stirred for 3 hours. The resulting solution, which contained the C-terminally amidated peptide, was then extruded through the syringe into a 50 ml centrifuge tube (Fisher, Toronto ON). The peptide was then precipitated with the addition of 50 ml of -20°C diethyl ether, and the tube was incubated at -80°C overnight. The precipitate was then pelleted by centrifugation at -4°C, 4,000 rpm, 5 min, the supernatant removed, and two further ether precipitations were performed, each for 4 hours. The resulting pellet was air-dried overnight, and re-suspended in double distilled water with 0.1 % TFA (Sigma-Aldrich Co.).

Purification of both peptides was carried out by Donna Jackman (Biochemsitry Department, Memorial University) using high-pressure liquid chromatography (HPLC)(Varian ProStar HPLC, Varian Inc., St. Laurent, QC). The HPLC was equipped with a reverse-phase DYNAMAX C-8 preparatory column (Varian Inc., St. Laurent, QC), and peptides were eluted at a wavelength of 215 nm using an acetonitrile gradient (80/20% HPLC grade water/acetonitrile – 0/100% acetonitrile; Sigma-Aldrich Co). The mass of each peptide was confirmed by Lidan Tao (Genomics and Proetomics Facility,

Memorial University) with matrix assisted laser desorption ionization – time of flight mass spectrometry [MALDI-TOF MS – Genomics and Proteomics (GaP) facility, Memorial University]. Final purity of the peptides was determined to be >95% by analytical HPLC. Upon mass confirmation, the C-terminally amidated GAD-1 and GAD-2 putative mature peptides were lyophilized.

2.10. Circular dichroism (CD) spectroscopy

The secondary structure of GAD-1 and GAD-2 putative mature peptides was assessed in aqueous and lipid environments using circular dichroism (CD) spectroscopy. For liposome preparation, lyophilized 1-palmitoyl-2-oleoyl-*sn*-glycero-3-phosphocholine (POPC) and 1-palmitoyl-2-oleoyl-*sn*-glycero-3-phospho-(1'-rac- glycerol) (POPG) [Avanti Polar Lipids Inc, Alabaster, Al] were dissolved separately in 20 mM pH 5 dibasic phosphate buffer to a concentration of 25 mM, and subjected to five freeze-thaw cycles. The resulting liposome solutions were extruded through a 200 nm filter (Nuclepore track-etch membrane, Whatman, Toronto ON) under nitrogen gas pressure. In addition, CD was used to assess secondary structure in the presence of 25 mM sodium dodecyl sulphate (SDS, Sigma-Aldrich Co.). A Jasco J-810 spectropolarimeter (Jasco Inc., Easton, MD) was used to assess secondary structure of GAD-1 and GAD-2 in buffer, as well as in the presence of 20 % TFE and POPC and POPG liposomes. Spectra were collected (20 for each analysis) in the far ultraviolet range, and were recorded using a 1 mm quartz cuvette. Spectra were collected between 193 and 260 nm. For both GAD-1 and GAD-2, four separate solutions were made: 1) 30 μM peptide in 20 mM pH 5 dibasic

phosphate buffer, 2) 30 μM peptide in 20 mM pH 5 dibasic phosphate buffer with 20 % TFE, 3) 30 μM peptide in 20 mM pH 5 dibasic phosphate buffer with addition of 1 mM POPC liposomes, and 4) 30 μM peptide in 20 mM pH 5 dibasic phosphate buffer with addition of 1 mM POPG liposomes. It should be noted that the same peptide stock solution was used for CD analysis of each peptide and, thus, CD data would be directly comparable for each of GAD-1 and GAD-2 (except for SDS, which used a different stock solution and must be taken as a strict estimate). Stock solutions were prepared using the molecular mass of the peptide, and calculating the weight required, which was weighed accurately with an analytical balance. Secondary structural characteristics of GAD-1 and GAD-2 were estimated from the collected spectra following the method of Yang et al., 1986. This method compares CD spectra values to those of a set of known reference proteins (myoglobin, lactate dehydrogenase, lysoozyme, cytochrome *c,* subtilisin BPN, papain, ribonuclease A, α-chymotrypsin, elastase, and concanavalin A) with X-ray crystallography results, most of which have been studied by five laboratories. For helical proteins, Yang et al (1986) found that the difference between the CD and X-ray crystallography data used to determined helical fractions was 3-8 %.

2.11. Solution nuclear magnetic resonance (NMR)

Both putative mature GAD-1 and GAD-2 peptides were assessed structurally using nuclear magnetic resonance (NMR). Peptide samples (2 mM; synthesized as in section 2.9) were dissolved at pH 5 in a solution of 90% H_2O, 10% D_2O, 0.2 mM 4,4-dimethyl-4-silapentane-1-sulfonic acid (DSS), and 150 mM deuterated SDS (Cambridge

Isotope Laboratories, Andover, MA). Samples were loaded into a thin-walled glass NMR tube (Norell Inc. Landisville, NJ). For all experiments, DSS was used as an internal reference and the water-gate water suppression was used with a 3-9-19 pulse. All 2D experiments used a recycle delay of 1 second. For both GAD-1 and GAD-2, one dimensional (1D) and two-dimensional (2D) NOESY and TOCSY spectra were obtained using a Bruker Avance 600 MHz spectrometer equipped with a TXI probe. For 1D ^{1}H NMR, 16 scans were used. A mixing time of 150 ms was used with 472 scans for the 2D NOESY. For the 2D TOCSY, a DIPSI2 spin-lock sequence was used, and the mixing time was 80 ms, with 128 scans. Spectra were processed using either iNMR (http://www.inmr.net) or TopSpin (Bruker, Milton, ON) and analyzed with SPARKY (Goddard et al., 2005).

2.12. Minimal inhibitory concentration (MIC) assay

A minimal inhibitory concentration (MIC) assay was used to assess the antimicrobial activity of GAD-1 and GAD-2. Using the colony suspension method (Wiegand et al., 2008), 3-5 morphologically similar colonies of both JM109 *Escherichia coli* (Invitrogen) and *Staphylococcus intermedius* (American Type Culture Collection #29663, Manassas, VA) were picked with a sterile loop. The colonies were transferred to a sterile plastic capped tube containing sterile Mueller-Hinton broth (MHB, BD Diagnostics Co., Mississauga, ON), and vortexed to re-suspend. Turbidity of the solution was assessed spectrophotometrically, and was adjusted by adding more broth or bacterial material to obtain an OD at 625 nm in the range of 0.08-0.013, resulting in an inoculum

density of 1 x 10e8 colony-forming units (cfu)/ml. A further 1:200 dilution with MHB was performed to arrive at the working concentration of 5 x 10e5 cfu/ml.

Two 96-well round-bottom polypropylene plates (Corning Inc., Corning, NY) were used for the MIC assay. Lyophilized GAD-1 and GAD-2 were prepared in 20 mM phosphate buffer, pH 5, to obtain stock solutions at a concentration of 1 mg/ml, and 20 µl of these solutions were pipetted in duplicate into the wells of column 1 of plate 1. Also, 20 µl of the 20 mM phosphate buffer, pH 5, was added (column 1, plate 1) in place of the gaduscidins to determine any bactericidal effects of the buffer itself. Next, 20 µl of a 0.04 % acetic acid and 0.02 % bovine serum albumin solution (BSA, Sigma-Aldrich Co.) was added to the wells containing the AMPs as well as the buffer control (column 1, plate 1), and the resulting solutions were mixed by pipette. Subsequently, 10 µl of a 0.02 % acetic acid and 0.01 % BSA solution was added into all wells of columns 2-10 of plate 1. In order to obtain a two-fold dilution, 10 µl from each well in column 1 was then added to each corresponding well in column 2. This procedure was repeated for each row until column 10, and the last withdrawn solution from column 10 was discarded. The bacterial suspension adjusted to 5 x 10e5 cfu/ml (described above) was then added to plate 2; 90 µl was pipetted into columns 1-10, and 100 µl into column 11 for the growth control. For the sterility control, 100 µl of MHB was pipetted into the wells of column 12 of plate 2. Once both plates were set up as described above, 10 µl from each of the 10 wells containing peptide dilutions in plate 1 was added to its corresponding wells in plate 2. The plate (2) was then sealed with breathable sealing tape, and incubated in a shaking incubator at 37°C for 16 hours. To ensure valid results, the inoculation density used in the assay was reaffirmed. Briefly, a 10 µl aliquot was removed from the growth control well

immediately after inoculation of the plate, and pipetted into 990 µl of sterile MHB and mixed by vortexing. A further 1:10 dilution of this solution was made by pipetting 100 µl into 900 µl of MHB. Both of these inoculum dilutions were plated onto MHB-agar plates (BD Diagnostics Co.), and incubated at 37°C for 16 hours. The presence of 500 and 50 colonies on these plate dilutions corresponds to the correct density of 5 x 10e5 cfu/ml.

As stated in Wiegand et al., 2008, MIC should not be taken as correct if a pellet of 2 mm sediment in the growth control well is not observed, or if the sterility control is turbid. MIC of GAD-1 and GAD-2 is defined as in Wiegand et al., 2008 as the lowest concentration of each AMP that inhibits visible growth of the tested isolate as observed with visual inspection.

2.13. Hemolytic assay

The hemolytic assays were completed as in Stark et al., 2002, with minor modifications. Fresh blood was collected from an Atlantic cod specimen using a 10 ml syringe rinsed with heparin, centrifuged at 4°C for 5 min at 3,000 X g. The serum fraction was discarded and the volume was raised to the original blood volume with 150 mM NaCl (Sigma-Aldrich Co). The resulting solution was mixed by inversion, centrifuged at 4°C for 5 min at 3,000 X g. This washing procedure was repeated twice. Upon removing the NaCl after the last wash step, the volume was brought up again to the original whole blood volume with 100 mM sodium phosphate buffer, pH 7. The red blood cells (RBCs) were then diluted 1 to 10 with the phosphate buffer, which yields a RBC suspension of 5x10e8 RBC/mL. For the assay, two concentrations of each of GAD-

1 and GAD-2 (125 μg/ml and 7.81 μg/ml) were prepared in 15 ml conical tubes (Corning Inc) with 100 mM phosphate buffer, pH 5, in a volume of 800 μL. Then, 200 μl of the diluted RBC solution was added and then mixed by inversion. The tubes were then placed in a water bath at 37°C for 60 min, and mixed by inversion. For the positive control, 800 μL of 1% (v/v) Triton X-100 (Sigma-Aldrich Co) was added to 200 uL of the RBC solution, in order to induce bursting of all RBCs due to the difference in osmolarity. Also, RBC supernatants suspended in 100 mM phosphate buffer, pH 7, served as a 0% hemolysis negative control. After the water bath incubation, all samples were mixed by inversion and centrifuged at 4°C, 3, 000 X g for 5 min. The supernatants were collected in sterile microfuge tubes, and absorbance was measured at 541 nm (the characteristic wavelength of hemoglobin). Percent hemolysis was defined as:

% hemolysis = [(absorbance of sample – absorbance of negative control)/(highest absorbance for positive control)] X 100.

3. Results

3.1. *Identification of potential AMP-coding transcripts*

Identification of potential AMP-coding sequences began with mining the CGP EST database (http://codgene.ca, Bowman et al. in press). This database contains EST sequences from a number of tissues obtained using techniques such as suppression subtractive hybridization (SSH), which leads to "libraries" enriched for genes up-regulated or down-regulated in response to stimuli such as heat-shock or IP injection of PAMPs (e.g. bacterial antigens or viral mimic). Using the CGP EST search engine tool, I identified a potential antimicrobial AutoFACT (Koski et al., 2005) annotation on one of these sequences, GAD-1. The contig contained four ESTs (GenBank accession numbers FG315061, EY972641, EY973733, and EY974225) (Table 1, Supplemental Table S1) and encoded a putative AMP. Based on tBLASTn of contig all_v2.0.10048.C1 sequence against the CGP EST database (Bowman et al. in press), we identified a contig containing two ESTs (all_v2.0.3805.C2; accession numbers FF411786 and ES773100) (Table 1, Supplemental Table S1) representing a second, related cod AMP-like gene. In addition to GAD-1 and GAD-2, two additional putative AMP coding transcripts were also found by applying AMPer (Fjell et al., 2007), hidden Markov model based software to the CGP EST database. This program is designed to identify AMP sequence motifs by comparing input amino acid sequences to known AMPs that have been clustered by physicochemical properties such as hydrophobic fraction, charge, and length. Mining of the EST database with AMPer revealed two AMP-like transcripts: lipopolysaccharide binding protein (LBP), and a transcript with sequence similarity with snakin-2 from *Solanum tuberosum*. Both were assessed bioinformatically, and ten fold-coverage of the cDNA sequence of

the 3' end of the latter was obtained using by designing primers specific for the EST representing the snakin-2-like sequence, bi-directional RACE, and subsequent sequencing of cloned cDNA (according to materials and methods, Chapter 2). However, the cDNA sequence of the 5' end of the snakin-2-like transcript was not obtained, and the project moved ahead with transcript expression characterization of GAD-1 and GAD-2 exclusively.

3.2 GAD-1 and GAD-2 sequence identification

Starting from the contiguous DNA sequence identified "all_v2.0.10048.C1" in the CGP EST database (representing GAD-1, I then validated the putative translation of this sequence for AMP sequence motifs using the AMPer program (Fjell et al., 2007). The putative peptide aligned well (E-value 0.034) to AMPer prepropeptide database Cluster 3, whose representative member is chryosphosin from red sea bream (Iijima et al., 2003). Based on tBLASTn of contig all_v2.0.10048.C1 sequence against the CGP EST database (Bowman et al. in press), we identified a contig containing two ESTs (all_v2.0.3805.C2; accession numbers FF411786 and ES773100) (Table 1, Supplemental Table S1) representing a second, related cod AMP-like gene, GAD-2.

3.3. GAD-1 and GAD-2 cDNA sequence determination

The putative AMP-coding GAD-1 and GAD-2 sequences obtained from the CGP EST database were incomplete and, thus, I needed to obtain the full-length cDNA

sequence. In order to obtain these sequences, I designed RACE primers that were complimentary to each EST sequence in order to amplify the 3' and 5' ends of the transcript. In addition, these primers were designed to our PCR amplification temperatures, and length (Section 2.3 and Table 2). Using bi-directional RACE, I obtained the full-length cDNA sequences for GAD-1 (GenBank accession number HM015527) and GAD-2 (HM015528), which are 405 bp and 401 bp in length, respectively (Figure 3). Alignment of these two cDNA sequences revealed that they have 87% identity at the nucleotide level. In addition, the putative translations (Figure 3), of these nucleotide sequences were aligned, and have 61% identity at the amino acid level. For RACE, I used a cDNA template synthesized from pooled RNA from several individuals (see Methods); the sequencing of multiple GAD-2 clones revealed two single nucleotide polymorphisms (SNPs) at positions 128 (A-G) and 165 (T-C) (Figure 3). Although both SNPs were within the GAD-2 open reading frame (ORF), only the SNP at position 128 causes an amino acid change [glutamic acid (E) → glycine (G)] in the hypothetical peptide sequence. No SNPs were identified in the GAD-1 cDNA sequences.

The putative translations for GAD-1 and GAD-2 exhibited sequence similarity to members of the piscidin family in fish. The best Uniprot BLASTP hit for GAD-1 was striped bass moronecidin (Piscidin-1) (E = 7 e-4, 38% identity over 49 AAs), while the best BLASTP hit for GAD-2 was a piscidin-like peptide found in red-spotted grouper (E = 0.002, 54% identity over 35 AAs). The sequence similarities are shown in the multiple-sequence alignment (Figure 4). A molecular phylogenetic tree indicating the evolutionary relationships of GAD-1 and GAD-2 with AMPs from various other fish species is shown in Figure 5. GAD-1 and GAD-2 appear to be most closely related to the piscidin-like

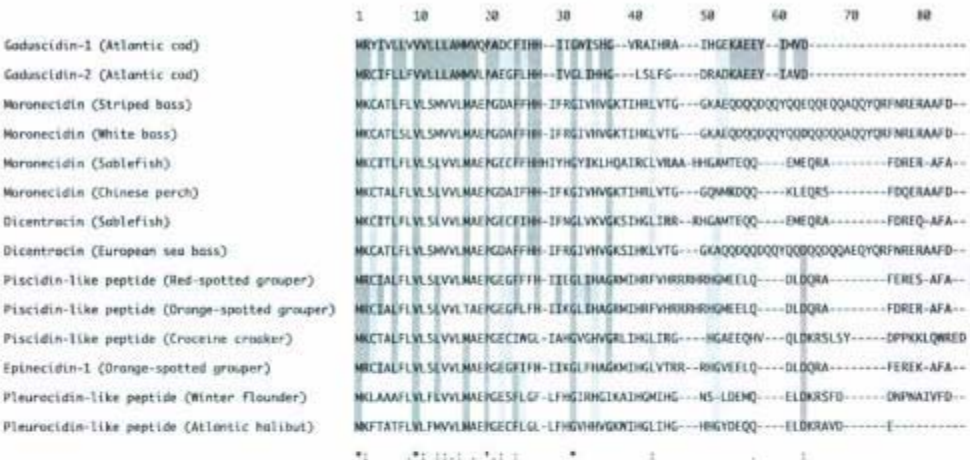
1 10 20 30 40 50 60 70 80
Gadascidin-1 (Atlantic cod)
Gadascidin-2 (Atlantic cod)
Moronecidin (Striped bass)
Moronecidin (White bass)
Moronecidin (Sablefish)
Moronecidin (Chinese perch)
Dicentracin (Sablefish)
Dicentracin (European sea bass)
Piscidin-like peptide (Red-spotted grouper)
Piscidin-like peptide (Orange-spotted grouper)
Piscidin-like peptide (Croceine croaker)
Epinecidin-1 (Orange-spotted grouper)
Pleurocidin-like peptide (Winter flounder)
Pleurocidin-like peptide (Atlantic halibut)

Figure 4. An amino acid sequence alignment of GAD-1 and GAD-2 with related sequences. The alignment was generated using the MegAlign ClustalW function (Lasergene 7.20). Asterisks were used to indicate identical residues, while colons and periods indicate conservative and semi-conservative residues (i.e. residues with similar physicochemical parameters), respectively. Identical residues in GAD-1 and GAD-2 sequences, as well as their best Uniprot BLASTP hits, are highlighted in dark grey. Identical residues between either GAD-1 or GAD-2 and related sequences are highlighted in light grey. The sequence names are followed by the common names of their species of origin. Following the sequence names, the scientific names for all species (in parentheses) and the GenBank and/or Uniprot accession numbers for these sequences are listed as follows: GAD-1 (*Gadus morhua*) HM015527; GAD-2 (*Gadus morhua*) HM015528; moronecidin (*Morone saxatilis*) Q8UUG0; moronecidin (*Morone chrysops*) Q8UUG2; moronecidin (*Anoplopoma fimbria*) C3KH06; moronecidin (*Siniperca chuatsi*) Q2VWH5; dicentracin (*Anoplopoma fimbria*) C3KHI8; dicentracin (*Dicentrarchus labrax*) P59906; piscidin-like peptide (*Epinephelus akaara*) B3VE23; piscidin-like peptide (*Epinephelus coioides*) B3VE24; piscidin-like peptide (*Larimichthys crocea*) B3VE22; epinecidin-1 (*Epinephelus coioides*) Q6JWQ9; pleurocidin-like peptide (*Pleuronectes americanus*) Q7T054; pleurocidin-like peptide (*Hippoglossus hippoglossus*) Q7SZG6.

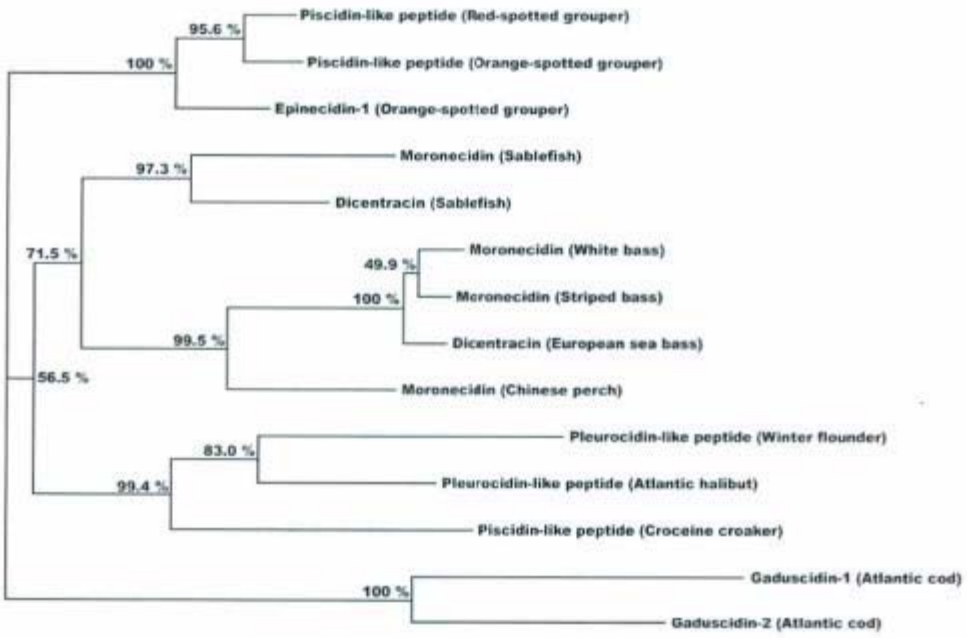

Figure 5. Molecular phylogenetic analysis of GAD-1 and GAD-2. The phylogenetic tree was generated using MEGA4 (Tamura et al., 2007) from the best GAD-1 and GAD-2 Uniprot BLASTP hits (E-values ≤ 1) as in Figure 4. The tree was bootstrapped 10,000 times, and these bootstrap values are shown as percentages.

peptides and epinecidin-1, and more distantly related to the moronecidins and dicentracins (Figure 5).

3.4. GAD-1 and GAD-2 constitutive mRNA expression

Upon obtaining full-length cDNA sequences for GAD-1 and GAD-2, QPCR primers were designed for transcript expression studies (e.g. to assess constitutive expression of these transcripts in a number of tissues). Paralogue-specific primers were designed to ensure that GAD-1 primers would not amplify GAD-2 and vice versa. QPCR data showed that there was high transcript expression variability between individuals for a given tissue. For example, in gill, the relative quantity values (RQs) of GAD-1 ranged from 4.5 in individual No. 6 to 789.5 in individual No. 4 (Fig. 4C, Supplemental Table S3A). In spleen, GAD-2 RQs ranged from 448.5 in individual No. 5 to 4,162.3 in individual No. 4 (Fig. 4D, Supplemental Table S3B). In some cases, high RQ in one tissue corresponded with high RQ in others; however, this generalization cannot be made for every individual (Figure 6). The expression of GAD-1 and GAD-2 transcripts was detectable in all 6 tissues examined in the constitutive expression study. However, the expression of these transcripts ranged widely across different tissues. The mRNA expression of GAD-1 and GAD-2 in spleen (the tissue with the highest expression of both GAD-1 and GAD-2) was 157.6 fold (for GAD-1) and 617.1 fold (for GAD-2) greater than their transcript expression in brain (the tissue with the lowest GAD-

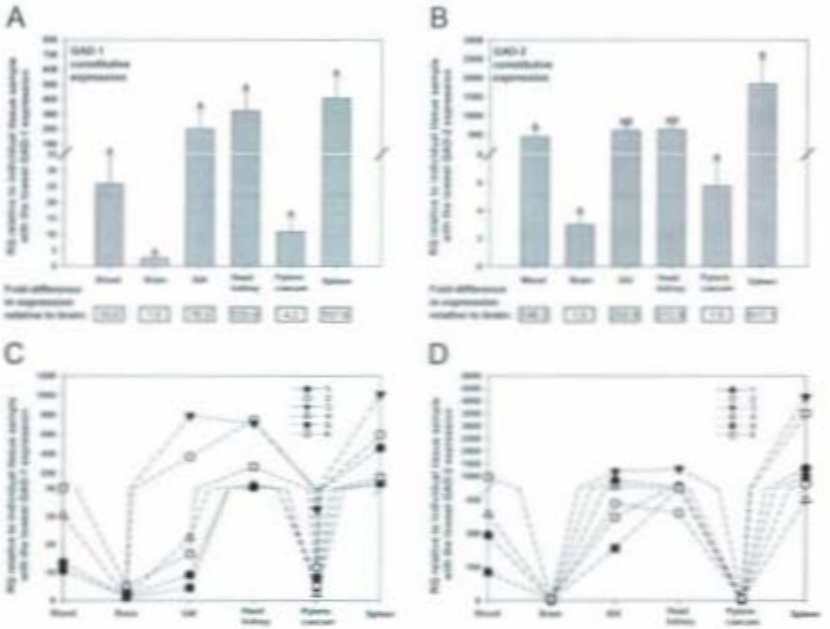

Figure 6. QPCR assessment of constitutive expression of GAD-1 (A) and GAD-2 (B) transcripts in multiple tissues. Expression data are presented as mean (± standard error) relative quantity (RQ) normalized to 18S ribosomal RNA. RQ values were calibrated to the individual with the lowest normalized GAD-1 or GAD-2 expression. Identical letters indicate no statistically significant difference in expression for each tissue comparison ($p > 0.05$). Expression for each tissue was calculated relative to the lowest expressing tissue (brain) as (average RQ for each tissue)/(average RQ for brain). RQ values for individual fish involved in the study are shown in panels C (GAD-1) and D (GAD-2) (Supplemental Table S3).

1 and GAD-2 transcript expression) (Figure 6A, B). GAD-2 mRNA expression in spleen was significantly ($p<0.05$) higher than in blood, pyloric caecum, or brain (Figure 6B, D).

3.5. GAD-1 and GAD-2 transcript expression response to bacterial antigens

After completing the multi-tissue constitutive expression analysis of GAD-1 and GAD-2, another QPCR study was carried out to assess any changes in expression upon bacterial antigen (ASAL) or saline injection (PBS). GAD-1 and GAD-2 transcripts were greater than 2-fold up-regulated (compared to the ASAL tank 0 h controls) by ASAL in spleen (Figure 7A,C) but not in head kidney (Figure 7B, D). For GAD-1, maximum ASAL response in spleen was observed at 2 HPI (3.6 fold up-regulated compared to 0 h; $p = 0.056$ for the 2 HPI versus 0 h ASAL groups), and transcript expression was significantly different ($p < 0.05$) in the 2 HPI and 24 HPI ASAL groups (Figure 7A). For GAD-2, maximum ASAL response in spleen was seen at 6 HPI (2.1 fold up-regulated compared to 0 h; $p = 0.129$ for the 6 HPI versus 0 h ASAL groups), and transcript expression was significantly different in the 6 HPI and 72 HPI ASAL groups (Figure 7C). In response to PBS injection, GAD-1 transcript was greater than 2-fold down-regulated in both spleen (5.7 fold compared to 0 h, no significant differences between PBS time points) and head kidney (2.8 fold compared to 0 h) at 6 HPI, and GAD-1 transcript expression in head kidney was significantly different between the PBS 6 HPI and 72 HPI groups

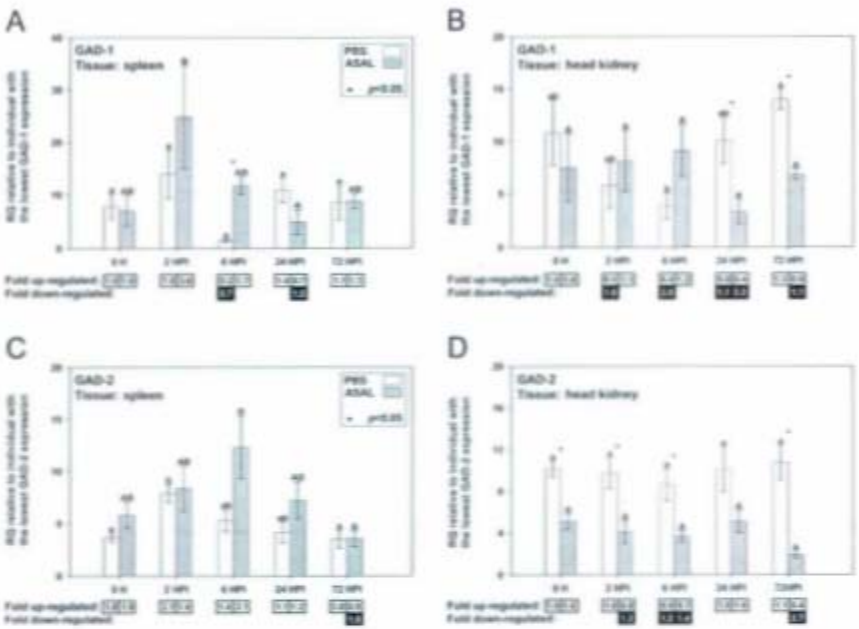
A
GAD-1
Tissue: spleen
PBS
ASAL
B
GAD-1
Tissue: head kidney
C
GAD-2
Tissue: spleen
D
GAD-2
Tissue: head kidney

Figure 7. QPCR analysis of GAD-1 (A, B) and GAD-2 (C, D) transcript expression in spleen (A, C) and head kidney (B, D) pre-injection (0 H) and at four time points after intraperitoneal injection of phosphate-buffered saline (PBS) or formalin-killed, atypical *A. salmonicidia* (ASAL). Expression data are presented as mean (± standard error) relative quantity (RQ) normalized to 18S ribosomal RNA. RQ values were calibrated to the individual with the lowest normalized GAD-1 and GAD-2 expression. Fold up-regulation for each injection time-point was calculated as (average RQ)/(average RQ for pre-injected control group). Down-regulation was calculated as the inverse of fold up-regulation if that value was less than one. Identical letters indicate no statistically significant difference in expression ($p > 0.05$) for each time-point post-injection within each treatment. Asterisks indicate a statistically significant difference ($p \leq 0.05$) between ASAL and PBS for a given time point. HPI = hours post-injection.

(Figure 7A,B). Interestingly, GAD-2 transcript was significantly up-regulated by PBS in spleen at 2 HPI (2.1 fold) compared to both 0 h and 72 HPI PBS groups (Figure 7C). In spleen, the transcript expression level of GAD-1 at 6 HPI was significantly different between PBS and ASAL groups (Figure 7A). In head kidney, the transcript expression level of GAD-1 was significantly different between PBS and ASAL groups at the 24 HPI and 72 HPI time-points (Figure 7B). For both ASAL and PBS groups in the GAD-2 head kidney study, there were no significant differences in transcript expression among different time points; however, the time-matched ASAL and PBS groups (with the exception of 24 HPI) were significantly different (shown by asterisks in Figure 7D) likely due to tank effect (i.e. GAD-2 was more highly expressed in individuals in the PBS tank prior to injection) rather than treatment effect.

3.6. Nodavirus carrier state and transcript expression of GAD-1 and GAD-2

Some individuals used in this study and previous studies were found to be asymptomatic carriers of nodavirus (Rise et al. 2008; Rise et al. 2010; Feng et al. 2009), and high nodavirus carrier state was shown to affect brain transcript expression for several immune-relevant genes (Rise et al., 2010). Nodavirus carrier state was determined by Charles Y. Feng (Ocean Science Center, Memorial University) in the brains of fish used in the study using a RT-PCR based method as in Rise *et al* (2008). Pixel intensity values (Supplemental Table S2) of RT-PCR bands generated using nodavirus-specific primers (Supplemental Figure S1) were analyzed. Individuals with no visible nodavirus RT-PCR band (mean pixel intensity in the range 662 to 5887), were

categorized as "no/low nodavirus", while individuals with visible nodavirus RT-PCR bands (mean pixel intensity in the range 10,973 to 33,733, see Supplemental Tables S2, S4, and S5) were categorized as "high nodavirus" for the purpose of statistical analyses. For brain (Supplemental Table S4) and immune tissues (spleen and head kidney, Supplemental Table S5), GAD-1 and GAD-2 transcript expression showed no significant differences ($p > 0.05$) between the no/low nodavirus group and the high nodavirus group. Therefore, high nodavirus carrier state did not significantly impact GAD-1 or GAD-2 mRNA expression in these tissues.

3.7. GAD-1 and GAD-2 mature peptide sequence and structure prediction

GAD-1 and GAD-2 transcripts encoded peptides that were 54 and 52 residues in length, respectively (Figure 3). However, AMPs are often translated as prepropeptides, and processed to the mature, active form. GAD-1 and GAD-2 sequences were input into the signalIP server (Nielsen et al., 1997; Bendtsen et al., 2004; http://www.cbs.dtu.dk/services/SignalP/), which predicts signal peptide cleavage at the same site, between amino acid residues 22-23. Prediction of the anionic pro-piece (the C-terminal residues of the prepropeptide; its cleavage yields the mature AMP) cleavage site was facilitated using sequence similarity and charge distribution comparisons with other known AMPs, and resulted in a cleavage of 11 residues from the N-terminus of both GAD-1 and GAD-2. Both pro-pieces had a net negative charge of -3, and shared 72% identity over 11 amino acids (ClustalW2; http://www.ebi.ac.uk/Tools/clustalw2/index.html).

A helical wheel model was used to determine amphipathicity of GAD-1 and GAD-2 putative mature sequences in an α-helical conformation. Using the University of California, Irvine Membrane Protein Explorer Version 3.2 helical wheel applet it was determined that both GAD-1 and GAD-2 could take on an amphipathic structure (Figure 8).

3.8. Circular dichroism (CD) spectroscopy

GAD-1 and GAD-2 putative mature peptides were chemically synthesized, and purified using HPLC. The strongest [highest absorbance in milli-absorbance units (mAU) at 215 nm] peak on each HPLC chromatograph (Section 2.9, Figures 9 and 10) was collected, and its mass analyzed using MALDI-TOF-MS. Initial efforts to solubilize the lyophilized GAD-1 and GAD-2 at physiological pH in dibasic phosphate buffer failed. Varying pH from 6 to 9, with and without the presence of salt (100 μM KCl) and/or cold also failed to dissolve the peptides. Finally, GAD-1 and GAD-2 dissolved in phosphate buffer at pH 5.

CD spectroscopy was carried out to estimate secondary structural characteristics of solubilized putative mature GAD-1 and GAD-2 in aqueous and membrane-mimetic environments. CD spectra of 30 μM GAD-1 and GAD-2 solutions were recorded at 25°C and pH 5 in aqueous solution, as well as in membrane-mimetic environments. Secondary structure content was estimated from the CD spectra following the method of Yang et al., 1986. The secondary structure of GAD-1 in aqueous solution, 20 mM dibasic phosphate buffer, was mostly random (6% α-helix, 27% ß-structure and 67% random coil)(Figure

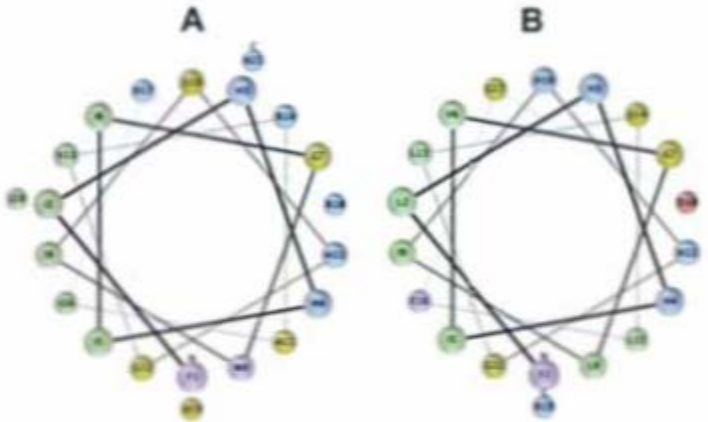

Figure 8. Helical wheel model of the first 18 residues of putative mature GAD-1 (A) and GAD-2 (B) generated using the University of California, Irvine Membrane Protein Explorer Version 3.2 helical wheel applet.

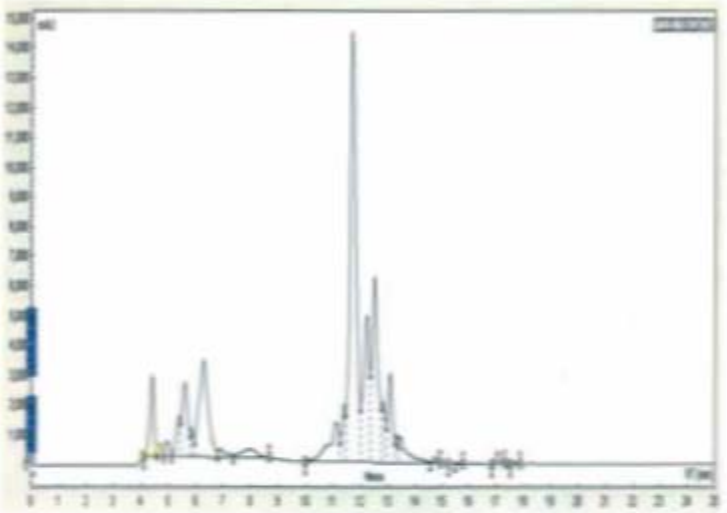

Figure 9. HPLC spectrum of GAD-1 eluted with an acetonitrile gradient. Samples were run through a reverse-phase HPLC chromatographer equipped with a preparatory DYNAMAX C-8 column. The strongest [highest absorbance in milli-absorbance units (mAU) at 215 nm] peak (~ 11.5 min) was extracted and confirmed to have a mass consistent with GAD-1 by MALDI-TOF-MS.

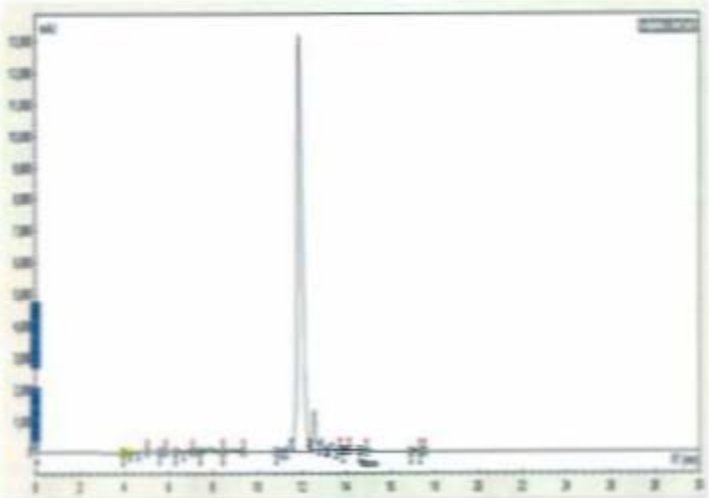

Figure 10. HPLC spectrum of GAD-2 eluted with an acetonitrile gradient. Samples were run through a reverse-phase HPLC chromatographer equipped with a preparatory DYNAMAX C-8 column. The strongest [highest absorbance in milli-absorbance units (mAU) at 215 nm] peak (~ 12 min) was extracted and confirmed to have a mass consistent with GAD-2 by MALDI-TOF-MS.

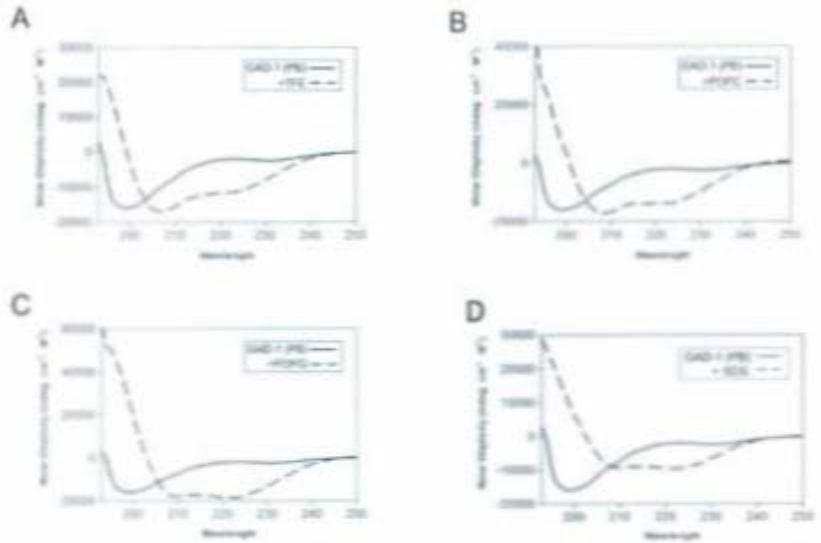

Figure 11. CD spectra of 30 μM GAD-1 dissolved in 20 mM pH 5 dibasic phosphate buffer as well as in the presence of A) 20 % TFE, B) 1 mM 200 nm diameter POPC liposomes, C) 1 mM 200 nm diameter POPG liposomes (See section 2.10 for liposome preparation), and D) 1 mM SDS liposomes. All spectra were taken using a 1 mm path-length quartz cuvette from 193 nm to 300 nm at 25°C.

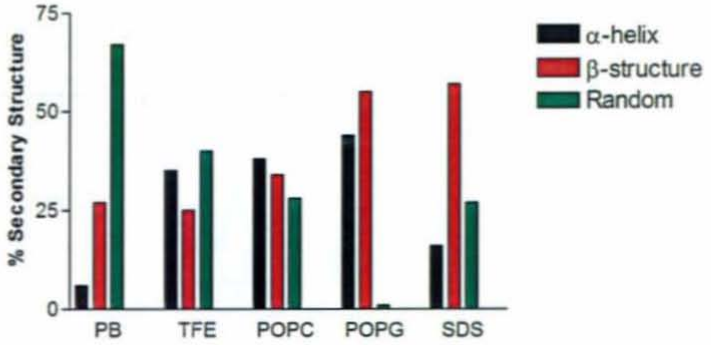

GAD-1	α-helix	β-structure	Random
PB	6	27	67
TFE	35	25	40
POPC	38	34	28
POPG	44	55	1
SDS	16	57	27

Figure 12. Graphical representation and corresponding percentage of secondary structural characteristics of 30 μM GAD-1 dissolved in 20 mM pH 5 dibasic phosphate buffer (PB), as well as in the presence of 20 % TFE, 1 mM 200 nm diameter POPC liposmes, 1 mM 200 nm diameter POPG liposomes, and 1 mM SDS liposomes. Note that CD with SDS was performed using a different stock solution and, thus, cannot be compared directly to other conditions. The structural content of α-helix, β-structure (a combination of β-turn and β-sheet), or random coil was calculated from the CD spectra data (Figure 11, section 2.9) as in Yang et al., 1986.

11A, 12). In the presence of 20% TFE, the α-helical content increased to 35% (25% ß-structure and 40% random coil)(Figure 11A, 12). In 1 mM 200 nm POPC liposomes, a zwitterionic membrane-mimetic environment, α-helical and ß-structure was increased to 38% and 34%, respectively (28% random coil)(Figures 11B, 12). The presence of anionic (POPG) liposomes appeared to increase α-helical and ß-structure (44% α-helix, 55% ß-structure and 1% random coil)(Figures 11C, 12) even more so than the zwitterionic (POPC) liposomes. The presence of SDS decreased the random structure when compared to phosphate buffer, but α-helix content of GAD-1 is lower in the presence of SDS as compared to all other membrane mimetics (Figure 11D, 12).

The composition of GAD-2 was largely random coil in aqueous solution (3% α-helix, 25% ß-structure and 72% random coil)(Figures 13A, 14) as well as in the presence of 20% TFE (4% α-helix, 25% ß-structure and 71% random coil)(Figures 13A, 14), and anionic (POPG) liposomes (5% α-helix, 32% ß-structure and 62% random coil)(Figures 13C, 14). However, the presence of POPC liposomes induced a structural change, which moderately increased α-helical content of GAD-2 (17% α-helix, 26% ß- It structure and 57% random coil)(Figures 13B, 14). Interestingly, in the presence of SDS, α-helix content of GAD-2 remains similar to that of other membrane mimetics. However, the presence of SDS induced a propensity toward ß-structure (Figure 13D, 14).

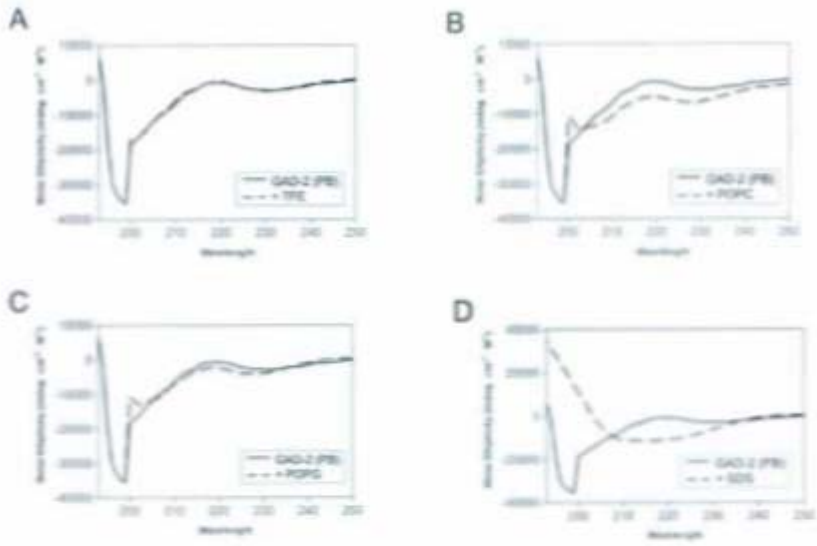

Figure 13. CD spectra of 30 μM GAD-2 dissolved in 20 mM pH 5 dibasic phosphate buffer as well as in the presence of A) 20 % TFE, B) 1 mM 200 nm diameter POPC liposomes, C) 1 mM 200 nm diameter POPG liposmes (See section 2.10 for liposome preparation), and D) 1 mM SDS liposomes. All spectra were taken using a 1 mm path-length quartz cuvette from 193 nm to 300 nm at 25°C.

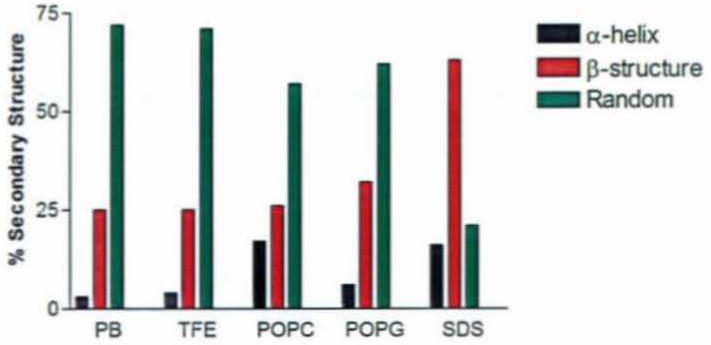

GAD-2	α-helix	β-structure	Random
PB	3	25	72
TFE	4	25	71
POPC	17	26	57
POPG	6	32	62
SDS	16	63	21

Figure 14. Graphical representation and corresponding percentages of secondary structural characteristics of 30 μM GAD-2 dissolved in 20 mM pH 5 dibasic phosphate buffer (PB), as well as in the presence of 20 % TFE, 1 mM 200 nm diameter POPC liposmes, 1 mM 200 nm diameter POPG liposomes, and 1 mM SDS liposomes. Note that CD with SDS was performed using a different stock solution and, thus, cannot be compared directly to other conditions. The structural content of α-helix, β-structure (a combination of β-turn and β-sheet), or random coil was calculated from the CD spectra data (Figure 13, section 2.9) as in Yang et al., 1986.

3.9. Preliminary solution nuclear magnetic resonance (NMR) structural characterization of GAD-1 and GAD-2

NMR studies were carried out to assess structural characteristics of GAD-1 and GAD-2 in a membrane-mimetic environment (SDS micelles), and lay the foundation for future high-resolution structure determination. Peaks greater than 7.6 ppm were considered backbone while those less than 7.6 ppm were considered side-chain or aromatic. The HN region of the 1D ^{1}H NMR spectrum for GAD-1 displays 13 peaks that were dispersed over 7.1-9.0 ppm (Figure 15). NMR spectra of well structured proteins typically have HN peaks spread over 2 ppm or more, while the dispersion for unfolded proteins is much less, typically < 0.5 ppm (Wuthrich, 1986). Thus it appears that GAD-1 is well structured in SDS micelles. Similarly, the HN peaks of GAD-2 were dispersed over 6.8-8.8 ppm (Figure 16). Hence, both GAD-1 and GAD-2 appear to exhibit a fair degree of structuring. The number of peaks and dispersion seen in the HN-Ha region of the TOCSYs (~7-9ppm, and ~3.5-5 ppm) are also consistent with both peptides taking on a reasonably, well defined-structure (Figures 17 and 18).

NOESY experiments showed that GAD-1 has 12 HN-HN correlations indicating 12 pairs of HN atoms close to each other in space. Such short HN-HN distances often occur in helical structure (Wuthrich, 1986), and thus indicate that at least 13 GAD-1 residues are in α-helical confirmation (Figure 19). However, the GAD-2 NOESY showed only 7 HN-HN correlations (Figure 20), which indicates that GAD-2 has less helical character than GAD-1. As well as providing some preliminary structural data, these NMR spectra indicate that GAD-1 and GAD-2 will be amenable for future structural studies aimed at determining atomic resolution structures of these peptides.

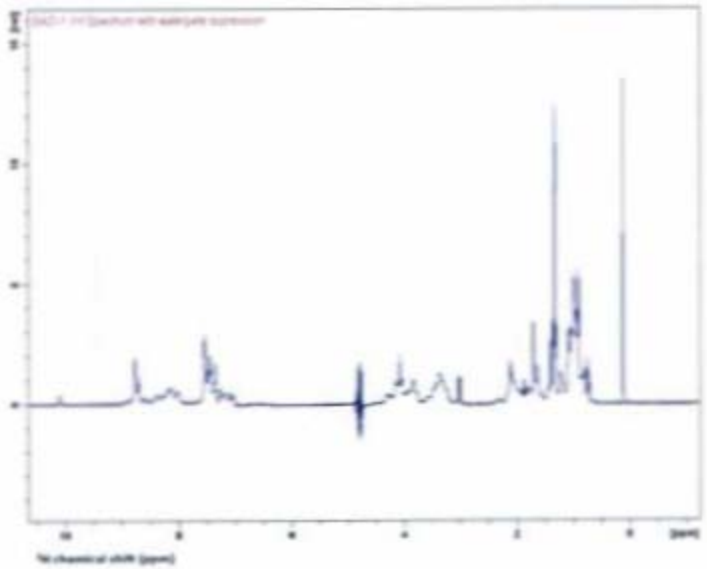

Figure 15. 1D solution NMR ^1H spectrum of GAD-1. The peptide sample (2 mM) was dissolved at pH 5 in a solution of 90% H_2O, 10% D_2O, 0.2 mM DSS, and 150 mM deuterated SDS. The spectrum was acquired with 16 scans and processed using Top Spin (Bruker).

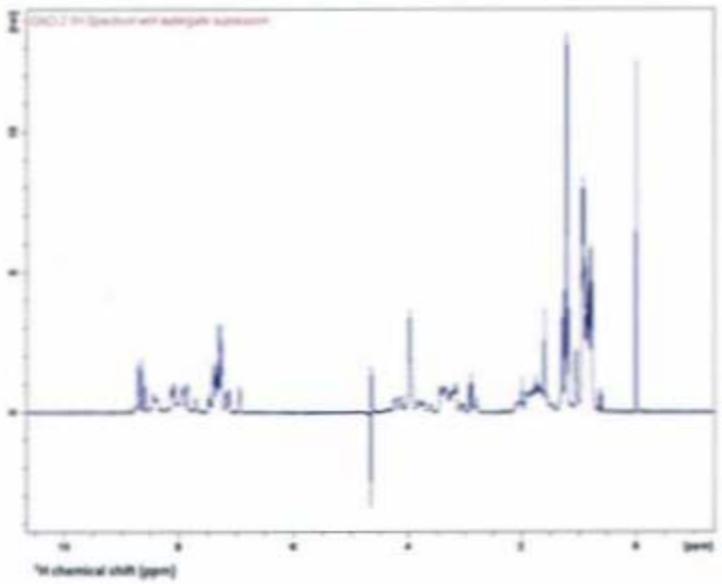

Figure 16. 1D solution NMR ^{1}H spectrum of GAD-2. The peptide sample (2 mM) was dissolved at pH 5 in a solution of 90% H_2O, 10% D_2O, 0.2 mM DSS, and 150 mM deuterated SDS. The spectrum was acquired with16 scans and processed using Top Spin (Bruker).

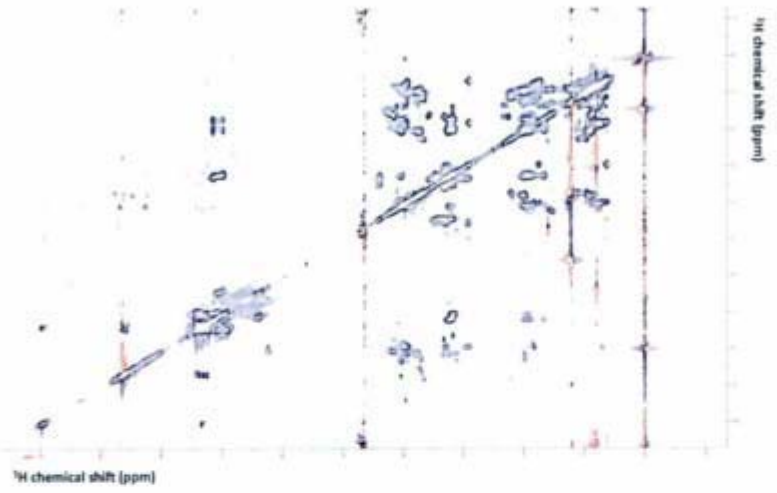

Figure 17. Solution NMR 2D TOCSY spectrum of GAD-1. The peptide sample (2 mM) was dissolved at pH 5 in a solution of 90% H_2O, 10% D_2O, 0.2 mM DSS, and 150 mM deuterated SDS. The spectrum was acquired with 128 scans and a mixing time of 80 ms. The processing was done using iNMR (http://www.inmr.net).

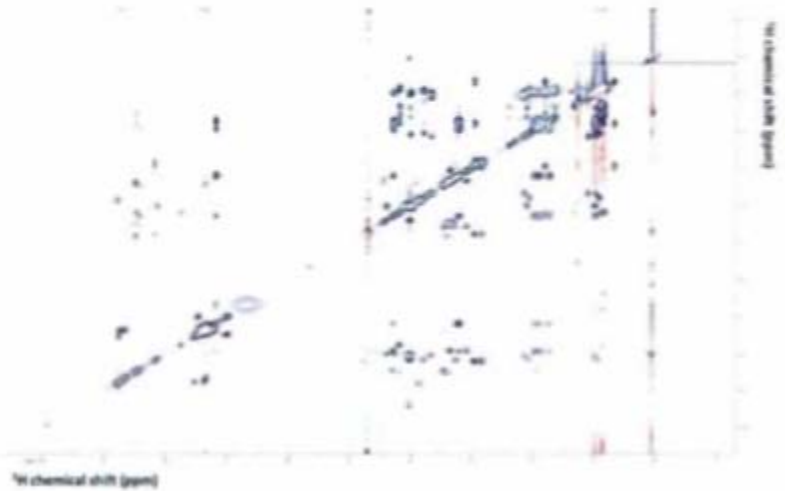

Figure 18. Solution NMR 2D TOCSY spectrum of GAD-2. Peptide samples (2 mM) were dissolved at pH 5 in a solution of 90% H2O, 10% D2O, 0.2 mM DSS, and 150 mM deuterated SDS. The spectrum was acquired with 128 scans and a mixing time of 80 ms. The processing was done using iNMR (http://www.inmr.net).

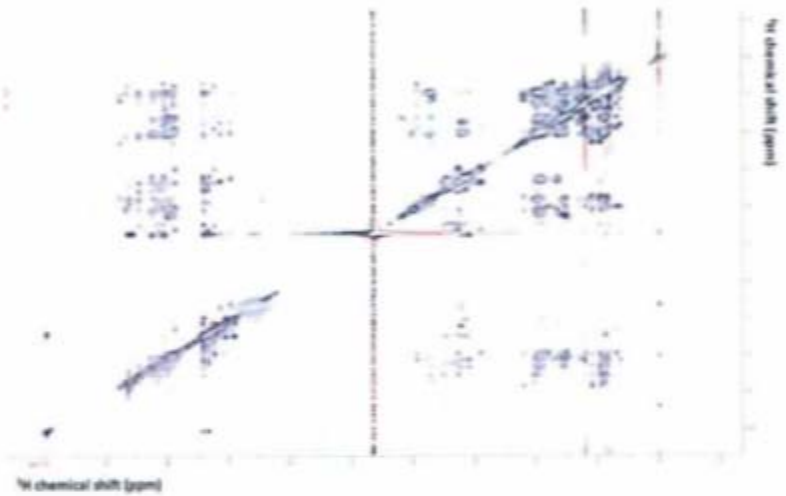

Figure 19. Solution NMR 2D NOESY spectrum of GAD-1. The peptide sample (2 mM) was dissolved at pH 5 in a solution of 90% H_2O, 10% D_2O, 0.2 mM DSS, and 150 mM deuterated SDS. The spectrum was acquired with 128 scans and a mixing time of 150 ms. The processing was done using iNMR (http://www.inmr.net).

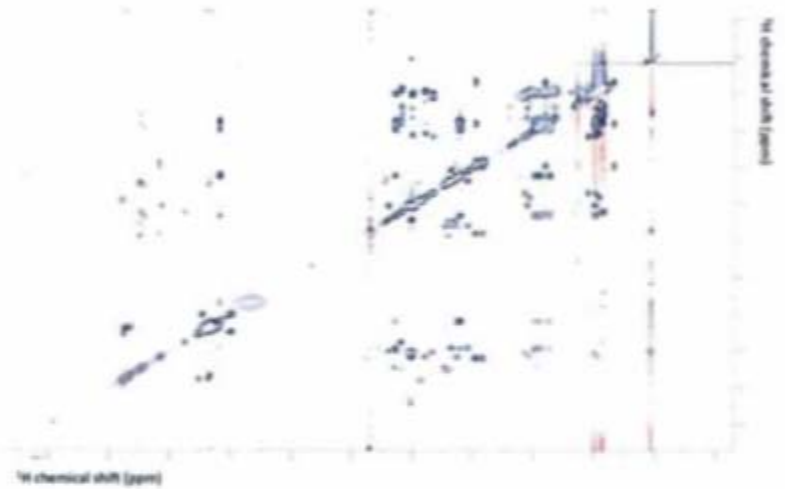

Figure 20. Solution NMR 2D NOESY spectrum of GAD-2. The peptide sample (2 mM) was dissolved at pH 5 in a solution of 90% H2O, 10% D2O, 0.2 mM DSS, and 150 mM deuterated SDS. The spectrum was acquired with 128 scans and a mixing time of 150 ms. The processing was done using iNMR (http://www.inmr.net).

3.10. Determination of minimal inhibitory concentration (MIC) for GAD-1 and GAD-2

To determine the antimicrobial efficacy of putative mature GAD-1 and GAD-2, an antimicrobial (MIC) assay was carried out. The MIC values of synthetic, C-terminally amidated GAD-1 and GAD-2 putative mature peptides were determined for a Gram-positive and Gram-negative species, *S. intermedius* and *E. coli*, respectively (Figure 21). GAD-1 was more potent in bacterial growth inhibition, with MIC values two-fold lower than GAD-2 for both bacterial species tested. (Table 3, Figure 21).

3.11. Determination of hemolytic activity of GAD-1 and GAD-2

To determine if putative mature GAD-1 and GAD-2 peptides had any effect on eukaryotic red blood cells (RBCs), hemolytic activity for both was determined. The results indicate that GAD-1 exhibited greater hemolytic activity than GAD-2 (Table 4). At 125 μg/ml, GAD-1 and GAD-2 induced 42% and 32% hemolysis, respectively. At a lower concentration (7.81 μg/ml), hemolytic activity of GAD-1 was still greater at 21 % compared to 14% for GAD-2 (Table 4).

Table 3. Results of antimicrobial susceptibility testing; GAD-1 and GAD-2 minimal inhibitory concentration (MIC) values with a Gram-positive and Gram-negative species.

	GAD-1 (μg/ml)[1]	GAD-2 (μg/ml)
Staphylococcus intermedius (+)	6.1 (± 3.1)	25 (± 12.5)
Escherichia coli (-)	12.5 (± 6.1)	50 (± 25)

[1]MIC determination and solution conditions for these AMPs can be found in section 2.11.

	1	2	3	4	5	6	7	8	9	10	11	12
GAD-1 *E. coli*	X	X	X	□	□	□	□	□	□	□	GC	SC
GAD-2 *E. coli*	X	□	□	□	□	□	□	□	□	□	GC	SC
GAD-1 *S. intermedius*	X	X	X	X	□	□	□	□	□	□	GC	SC
GAD-2 *S. intermedius*	X	X	□	□	□	□	□	□	□	□	GC	SC
Buffer Control	□	□	□	□	□	□	□	□	□	□	GC	SC

Figure 21. Graphical representation of the portion of a 96-well plate used for the MIC assay (Section 2.12). Note that an "X" represents no growth and a "□" represents normal growth (defined by Wiegand et al (2008) as being > 2 mm). GC represents the growth control and SC represents sterility control (Section 2.12).

Table 4. Results of GAD-1 and GAD-2 hemolytic assay using Atlantic cod red blood cells (RBCs).

	GAD-1 (%)[1]	GAD-2 (%)
Peptide conc. 125 µg/ml	42	32
Peptide conc. 7.81 µg/ml	21	14

[1] Determination of percent hemolysis of Atantic cod RBCs can be found in section 2.12.

4. Discussion

In this study, two AMP-like transcripts were identified in Atlantic cod by mining the CGP EST database. These paralogous transcripts were termed gaduscidins (GAD-1 and GAD-2), derived from the genus name of Atlantic cod, *Gadus*. GAD-1 and GAD-2 encoded putative AMPs that are 54 and 52 residues, respectively. Based on the sequences of GAD-1 and GAD-2, the multiple sequence alignment and phylogenetic analyses suggest that these AMPs belong to the piscidin family, while representing a distinct group of AMPs within this family (Figure 4 and 5). Using the CGP EST database, Fernandes et al. (2010) also published a short paper that described a cod piscidin transcript, which I identify to be GAD-1. However, Fernandes et al. (2010) did not study the expression of this Atlantic cod piscidin-like transcript. My thesis work also includes the identification of an additional cod piscidin transcript (GAD-2) that is likely paralogous to GAD-1 based on sequence similarity. Expression of both of these transcripts was assessed constitutively and upon bacterial or saline injection. In addition, the putative mature peptides were chemically synthesized and assessed structurally, and used in assays, which confirm that they indeed possess antimicrobial activity.

QPCR analysis revealed that GAD-1 and GAD-2 transcript expression was highest in spleen, head kidney, and gill, intermediate in peripheral blood, and lowest in pyloric caecum and brain. The high levels of constitutive mRNA expression in head kidney and spleen are consistent with the immune functions of these tissues in teleosts. Similarly, a previous study in hybrid striped bass also revealed high levels of moronecidin transcript expression in head kidney and spleen (Lauth et al., 2002). In addition to high levels of gaduscidin transcript expression in immune tissues, the

expression of these transcripts were also high in gill. Previous studies in winter flounder have localized pleurocidin transcripts and protein products in epithelial cells of the skin and intestine (Cole et al., 1997, 2000). Although I did not examine epithelial tissues other than gill for GAD-1 and GAD-2 transcript expression, it is possible that cod epithelial cells also synthesized the gaduscidin transcripts detected in gill. The high levels of gaduscidin mRNA expression in head kidney, spleen, and gill are also consistent with the recent findings by Ruangsri et al. (2010), who demonstrated high antimicrobial activities contained within the crude protein extracts from these tissues in Atlantic cod. Several previous studies have demonstrated AMP expression in immune cells of various species. For example, piscidin-1 and piscidin-3 from hybrid striped bass have been localized to mast cells (Silphaduang and Noga, 2001). Similarly, Mulero *et al* (2008) determined that piscidins are contained within the granules of circulating mast cells and acidicophilic granulocytes of gilthead seabream (*Sparus aurata*). In human, a small α-helical AMP, the cathelicidin hCAP18/LL37 is also produced in immune cells including natural-killer cells, mast cells, and neutrophils (Lai and Gallo, 2009). In light of these previous demonstrations of AMP expression in immune cells of various species, the expression of GAD-1 and GAD-2 transcripts in cod blood may likewise be due to the presence of gaduscidin transcripts in circulating immune cells. Interestingly, I found that GAD-2 mRNA was expressed in blood and head kidney at similar levels (148.2 and 212.8-fold higher than in brain, respectively), whereas there was a greater than 10-fold difference in GAD-1 mRNA expression in blood and head kidney (10.0 and 125.0-fold higher than in brain, respectively). This suggests an important role for GAD-2 in peripheral blood, a hypothesis that warrants further investigation.

Constitutive transcript expression of GAD-1 and GAD-2 varied greatly between individuals for the tissues tested (Figure 6C and D). In human, it has been shown that the transcript expression level of hepcidin exhibits high variation in expression phenotypes partially due to a variety of genetic factors (Bayele and Srai, 2009). For example, the polymorphic *cis*-acting non-coding regions of the hepcidin gene can result in differential regulation of hepcidin transcription by cytokines and transcription factors among individuals (Bayele and Srai, 2009). The high biological variation in GAD-1 and GAD-2 transcript expression observed in our QPCR study may likewise be attributed to genetic variations among individuals.

Upon completion of constitutive expression analysis, a bacterial antigen (ASAL) injection study was carried out to assess if the gaduscidin transcripts were inducible in immune relevant tissues by bacterial stimulation. The ASAL antigens used in this study were previously shown to strongly induce (~ 10 to 69-fold) other AMP-like transcripts (hepcidin and cathelicidin) in spleen and head kidney of Atlantic cod at the 24 HPI time point (Feng et al., 2009). However, the current study shows that GAD-1 and GAD-2 transcript expression was weakly induced (less than 4-fold) by ASAL at earlier time points (2 HPI and 6 HPI) in spleen, and non-responsive to ASAL in head kidney. The lack of strong up-regulation of gaduscidin transcripts by ASAL stimulation is not without precedent, as similar results have been observed in previous studies. In hybrid striped bass, a lack of significant up-regulation of moronecidin transcripts following stimulation with *Streptococcus iniae* challenge was previously observed (Lauth et al., 2002). In mussel (*Mytilus galloprovincialis*), it was shown that while *Vibrio splendidus* injection decreased the background expression of mytilin AMP mRNA (Cellura et al., 2007), an

injection with a different bacterial species (*Vibrio anguillarum*) induced mytilin mRNA expression (Cellura *et al* 2009). It is possible that the inducibility of GAD-1 and GAD-2 transcripts may vary depending on the species of bacterial used to generate the antigen for stimulation. It is also reasonable to suspect that injection of live, virulent pathogens may have very different effects on GAD-1 and GAD-2 expression than injection of the formalin-killed bacteria used in the current study. Another possibility for the lack of ASAL induction is that the expression of Atlantic cod gaduscidins may be governed by post-transcriptional regulatory mechanisms. Similarly, post-translational modifications may also play an important role in the expression regulation of these AMPs as they are often translated with a signal peptide and pro-piece, which are enzymatically-cleaved to yield the mature peptide. Therefore, the expression and activity of AMPs are also highly dependent on the expression of certain proteases (Lai and Gallo, 2009).

While bacterial challenge has been shown to cause AMP transcript induction, these AMPs may be subject to regulation at the protein level as well. Similarly, the abundance of a particular AMP transcript may not correlate with the level of the prepropeptide, or the level of the active, mature AMP, in the tissue (Lauth et al., 2002). It has also been shown that precursor forms of AMPs can be stored at high concentrations in intracellular granules for release when needed (Lai and Gallo 2009), which also provides another possible regulatory mechanism for gaduscidin expression. Although GAD-1 and GAD-2 transcripts in spleen appear to be only weakly induced by ASAL stimulation, the high constitutive levels of these transcripts in immune-relevant tissues (e.g. spleen, head kidney, and blood) argue for potentially important immune functions

for gaduscidins. Thus, it is important that the mechanisms involved in regulation of these cod putative AMPs are elucidated.

Expression of immune-relevant genes in Atlantic cod brain can be affected by asymptomatic nodavirus carrier status (Rise et al., 2010). Therefore, we investigated if high nodavirus carrier state influenced GAD-1 or GAD-2 transcript expression in brain and immune-relevant genes. Viruses within the family Nodaviridae have been responsible for serious disease outbreaks in many species of marine fish (Chia et al., 2009). Upon exposure to this RNA virus, some fish can survive and become asymptomatic carriers. Chia *et al.* (2009) showed that two AMPs, tilapia (*Oreochromis mossambicus*) hepcidin 1-5 and cyclic shrimp (*Oenaeus monodon*) anti-lipopolysaccharide factor, exhibited antiviral activity against grouper nervous necrosis virus (GNNV) *in vitro*. Previous studies have shown that some of the fish used in our study were asymptomatic carriers of Atlantic cod nervous necrosis virus (ACNNV) (Rise et al., 2008; Feng et al., 2009; and Rise et al 2010). In addition, while asymptomatic high nodavirus carrier state had no significant effect on the basal expression of 13 immune-relevant transcripts in spleen (Rise et al., 2008), it had significant impact on the expression of several immune-relevant transcripts in brain (Rise et al., 2010). Therefore, it was important to determine if nodavirus carrier state influenced constitutive GAD-1 or GAD-2 transcript expression. Our analysis demonstrated that there was no statistically significant effect of high nodavirus carrier state on constitutive transcript expression of GAD-1 or GAD-2 in head kidney or spleen (Supplemental Figure S1, Supplemental Table S2). As previously noted, a similar result was observed in a study showing that high nodavirus carrier state in the brain had no statistically significant effect on the basal

expression of 13 immune genes in spleen (Rise et al., 2008). In addition, constitutive GAD-1 and GAD-2 transcript expression in brain was not significantly affected by high nodavirus carrier state. Therefore, the nodavirus carrier state of individuals involved in the QPCR studies presented in this thesis did not appear to influence the transcript expression results.

Upon completion of GAD-1 and GAD-2 nucleotide sequence characterization and various transcript expression studies, the study continued with the prediction of mature GAD-1 and GAD-2 peptide sequences, and chemical synthesis of both. Members of the piscidin family such as moronecidin and diacentracin (Cole et al., 1997; Lauth et al., 2002), are translated as prepropeptides, and processed to the mature, active form and, thus, it can be expected that GAD-1 and GAD-2 are processed in a similar manner. Processing of full-length AMPs often involves 1) signal peptide cleavage at the N-terminus, and 2) enzymatic cleavage of the C-terminal anionic pro-piece. Thus, bioinformatics sequence comparisons with known piscidin family members, and signal peptide cleavage site prediction using Signal IP were carried out. Using this tool, I predicted that the signal peptide cleavage site on both gaduscidins was at the N-terminal side of the phenylalanine at residue 22, which corresponds to the signal peptide cleavage sites for moronecidin and diacentracin (Cole et al., 1997; Lauth et al., 2002). Cleavage of the anionic pro-piece was also predicted by bioinformatics sequence comparisons with other fish AMPs. Thus, putative mature GAD-1 (FIHHIIGWISHGVRAIHRAIH), and GAD-2 (FLHHIVGLIHHGLSLFGDR) were 21 and 19 residues long, respectively, and are 42 % identical over 21 amino acids. Putative mature GAD-1 was isoleucine (28.6%) and histidine (23.8%) rich, while putative mature GAD-2 also appeared to be histidine-

rich (21.1%), but was interestingly leucine-rich (21.1%). It should be noted that the signal peptide and pro-piece cleavage sites reported here are merely predictions, and *in vivo* isolation of mature GAD-1 and GAD-2 is necessary to confirm the active AMP sequences. In addition, our chemical synthesis resulted in C-terminal amidation of GAD-1 and GAD-2. Although piscidins isolated *in vivo* are often C-terminally amidated (Chekmenev et al., 2006), isolation of GAD-1 and GAD-2 would be required to confirm any post-translational modifications.

Both putative mature peptides exhibited amphipathic characteristics when modeled as an α-helical structure, with hydrophobic and hydrophilic amino acids on opposite sides of the projection (Figure 8). This configuration was also observed in a helical-wheel projection of mature moronecidin (Lauth et al., 2002), and winter flounder pleurocidin (Cole et al., 1997), suggesting a similar configuration for putative mature GAD-1 and GAD-2. To confirm the prediction of an amphipathic α-helical structure, characterization of both putative mature GAD-1 and GAD-2 was also carried out.

CD and NMR spectroscopy were carried out to determine secondary structural characteristics of GAD-1 and GAD-2 putative mature peptides. CD analysis of GAD-1 indicates that it adopts a predominantly random coil structure in aqueous solution, but adopts a conformation greater in α-helical and β-structure in the presence of TFE, as well as zwitterionic (POPC) and anionic (POPG) membrane-mimetic environments (Figures 11, 12). TFE, known to promote α-helical structure in proteins (Myers et al., 1998 and references therein), also induced greater α-helical content in GAD-1 as compared to aqueous solution (Figures 11, 12). Membrane-mimetic environments, consisting of

zwitterionic (POPC) and anionic (POPG) liposomes also induced structural changes, increasing α-helical structure even more so than TFE, but also increased β-structure as compared to aqueous solution. 1D ^{1}H and 2D TOCSY NMR spectra also indicate GAD-1 is structured in the presence of a membrane mimetic (deuterated SDS; Figure 15 and 17). In addition, 2D NOESY NMR experiments demonstrated that GAD-1 adopts an α-helical structure at least 13 residues in length (Figure 19). Similarly, Chekmenev et al. (2006) determined that C-terminally amidated piscidin-1 and piscidin-3 take on an α-helical conformation in the presence of a 1:3 PC: PG membrane-mimetic environment. The charge of the lipid head-group has an impact on the secondary structural composition of GAD-1, as both α-helical structure and β-structure was greater in the presence of anionic (POPG) liposomes as compared to zwitterionic (POPC) liposomes (Figures 11, 12). Interestingly, in the presence of POPG, GAD-1 was almost entirely (99%) structured (Figure 12B) and exhibited a 20% increase toward β-structure in the presence of POPG as compared to POPC. This suggests a strong interaction with an anionic membrane such as those found in *Staphylococcus aureus* and *Bacillus subtilis* (Epand et al., 2009). This is in contrast to a zwitterionic membrane-mimetic environment (POPC), where GAD-1 was still 28% random coil; this observation may indicate a lesser interaction with membranes such as human RBCs, which are composed of zwitterionic phospholipids such as POPC (Gul et al., 1970).

GAD-2, however, remained primarily random coil in aqueous solution, as well as in the presence of TFE and anionic POPG liposomes (Figures 13, 14). GAD-2 α-helical content increased moderately in a zwitterionic (POPC) membrane-mimetic environment, but secondary structure was largely limited to β-structure, which was low (~25%) when

compared to random coil content (~70%)(Figure 14B). 1D ^{1}H and 2D TOCSY NMR experiments indicated that GAD-2 is structured in the presence of deuterated SDS (Figures 16 and 18); however, the 2D NOESY indicates that it had less α-helical character than GAD-2 with a helix prediction of at least 8 residues (Figure 20). When comparing secondary structural characteristics in aqueous and membrane-mimetic environments, GAD-2 did not exhibit a marked structural change as observed with GAD-1. However, studies using different membrane mimetics or varying physicochemical parameters may have different effects on GAD-2 structure.

It should be noted that our CD data for GAD-1 and GAD-2 in the presence of SDS does not agree with NMR results. Although a different stock solution of peptide was used, the helical content should be comparable to that of our NMR data. Thus, running the NMR sample itself will allow the identification of the discrepancy, and this will be the focus of a future study.

Although GAD-1 and GAD-2 are encoded by paralogous genes and share nucleotide and amino acid sequence similarity, it is evident that these peptides exhibit very different structural characteristics in their mature form. It is likely that the marked structural change observed with GAD-1 in aqueous versus membrane-mimetic environments will lead to GAD-1 exhibiting greater antimicrobial activity than GAD-2. Also, CD and NMR spectroscopy indicated that GAD-1 exhibited more α-helical character, and had an α-helix of greater length than GAD-2. Although further NMR studies are required to elucidate the mechanism by which GAD-1 and GAD-2 disrupt membranes (Figure 1), it is likely that GAD-2 does not conform to the barrel-stave mechanism, as this mechanism requires that the peptide spans the entire length of the

membrane (~30 Å; Rozek et al., 2000). However, it is possible that GAD-2 may form a dimer to span the membrane, similar to that of the 15-residue gramicidin from *Bacillus brevis* (Arseniev et al., 1985). Even though our preliminary NMR analysis revealed that both GAD-1 and GAD-2 were structured in a membrane-mimetic environment, further NMR studies are required to determine the three dimensional (3D) structure with atomic resolution. Using ^{1}H-NMR Campagna et al. (2007) determined that piscidin-1 likely permeabilizes DMPC membranes in a manner similar to the toroidal-pore mechanism (Figure 1C). Due to sequence similarity between piscidin-1 and the gaduscidins, is possible that GAD-1 and GAD-2 may conform to the toroidal-pore mechanism; however, more NMR experiments are required to further investigate this.

It was also determined by CD and ^{15}N solid-state NMR, that piscidin-1 in a 3:1 molar ratio of dimyristoylphosphatidylcholine (DMPC) and dimyristoylphosphatidylglycerol (DMPG) lies nearly in the plane of the bilayer where it adopts an α-helical structure (Chekmenev et al., 2006). Similarly, Fu et al (2009) used 2D ^{1}H-^{15}N-heteronuclear correlation NMR spectroscopy with piscidin-1 and a 3:1 molar ratio of DMPC and DMPG to show that amide protons from the hydrophilic side of piscidin-1 ^{15}N-LYS14 (an α-helical piscidin-1 analogue) interact with protons from water molecules at the bilayer surface, indicating that the AMP interacts with the aqueous environment when bound to the lipid bilayer. My CD and NMR results also indicate that GAD-1 and GAD-2 (to a lesser extent) are α-helical in the presence of membrane-mimetics, and these peptides share sequence similarity with piscidin-1. However, broader structural studies are required to further elucidate their orientation in the membrane, as well as the mechanism by which these peptides disrupt membranes.

Structural studies are an important primary step in ascertaining the mechanism of an AMP. However, functional assays were needed to confirm that GAD-1 and GAD-2 possess antimicrobial activity. To assess antimicrobial efficacy against a Gram-positive and Gram-negative bacterial species, MIC functional assays were carried out using both gaduscidins. It was determined that C-terminally amidated putative mature GAD-1 and GAD-2 both exhibited antimicrobial activity against *S. intermedius* (Gram-negative) and *E. coli* (Gram-positive). GAD-1 MIC values were two-fold lower than those of GAD-2 in the case of both species analyzed, indicating that it may be a more potent AMP. Other members of the piscidin family have comparable antimicrobial activities with the gaduscidins. For example, MIC values against *E. coli* for hybrid striped bass piscidin-1 and piscidin-3 were both 3.1 μg/ml (Silphaduang and Noga, 2001), compared to 12.5 μg/ml for GAD-1, and and 50 μg/ml for GAD-2. However, hybrid striped bass piscidin-4 exhibited comparable antimicrobial activity to GAD-2 (50 μg/ml), and less activity than GAD-1 in a MIC assay using *E. coli* (Noga et al., 2009). In the case of *Staphylococcus aureus*, piscidin-1 and piscidin-3 MIC values were 3.1 μg/ml, while piscidin-4 values ranged from 6.3-12.5 μg/ml. GAD-1 and GAD-2 exhibited MIC values of 6.1 and 25 μg/ml respectively against another *Staphylococcus* species (*S. intermedius*); however, *S. aureus* was not tested. Although gaduscidin AMP sequences are quite divergent from other fish species (Figure 4 and 5), they still have potent antibacterial activity against the two bacterial species tested.

GAD-1 and GAD-2 exhibit less antimicrobial activity than other piscidin family members, but appear to be more effective in activity than frog AMPs, and are comparable in activity to wasp (Xu et al., 2005) and human (Sass et al., 2008) AMPs. The aurein

AMPs, derived from secretions from the granular dorsal glands of the green and golden bell frogs, *Litoria aurea* and *Litoria raniformis*, respectively exhibit MIC values of 50 μg/ml against *S. aureus, Staphylococcus epidermidis, and Streptococcus uberis* (Rozek et al., 2000; Apponyi et al., 2004). Conlon et al., (2008) determined that numerous AMPs isolated from skin secretions of hose's rock frog, *Odorrana hosii*, have MIC values of 62.5 μg/ml or greater when tested against *E. coli* and *S. aureus*. AMPs derived from wasp (*Vespa magnifica*) venom are comparable in activity to GAD-1 and GAD-2, with MIC values of ranging from 7.5-30 μg/ml, against *E. coli* (Xu et al., 2005). In addition, vespid (wasp) AMPs exhibited MIC values in the range of 3.7-10 μg/ml against *S. aureus*. Human AMPs such as hBD-3 and hCAP18/LL-37 exhibit MIC values similar to those of lower vertebrate species. MIC values were determined to be 7.4 and 12.9 μg/ml against *S. aureus* for these human AMPs (hBD-3 and hCAP18/LL-37), respectively (Sass et al., 2008). Song et al. (2008) also determined that recombinant hBD-3 MIC value was >25 μg/ml against *E. coli* and, thus, GAD-1 has greater antimicrobial activity than this human AMP. Although an *in vitro* MIC assay is a good indication of antimicrobial activity, it is just one measure of AMP efficacy, and many other parameters are involved *in vitro*. For example, in the interest of survival, many bacterial species are known to adjust their membrane composition by metabolic means (Zhang et al., 2008). In addition, the vast number of bacterial species and varying membrane lipid composition between them further complicates the study of antimicrobial activity.

To assess if GAD-1 or GAD-2 putative mature peptides have any effect on eukaryotic cells, hemolytic assays were carried out using Atlantic cod RBCs. AMP-induced lysis of eukaryotic cells was observed with the addition of C-terminally amidated

putative mature GAD-1 and GAD-2. Both of these AMPs exhibited hemolytic activity against Atlantic cod RBCs. GAD-1 was more hemolytic than GAD-2, with 42% hemolysis of Atlantic cod RBCs at 125 μg/ml compared to 32% for GAD-2 at the same concentration. GAD-1 exhibited *E. coli* growth inhibition at a concentration of 12.5 μg/ml, and at a concentration of 7.81 μg/ml, exhibited 21% hemolysis. Thus, this AMP will affect RBCs at a comparable concentration to that required to inhibit *E. coli* growth. However, the MIC value against *S. intermedius* was 6.1 μg/ml, but would presumably kill eukaryotic cells at this concentration to a lesser extent than the 7.81 μg/ml resulting in 21% hemolysis. GAD-2 antimicrobial activity was less than that of GAD-1, but GAD-2 also exhibited less hemolytic activity (14% at 7.81 μg/ml). However, a GAD-2 concentration of 25 and 50 μg/ml is required to inhibit growth of *S. intermedius* and *E. coli*, respectively -four-fold higher than GAD-1 against the same bacterial species. Thus, it is evident that at a concentration required to kill these bacterial species, GAD-1 is less hemolytic than GAD-2.

GAD-1 and GAD-2 exhibited hemolytic activity comparable to other fish species. For example, C-terminally amidated, and non-amidated piscidin-1 at a concentration of 100 μg/ml exhibited 73 and 78 % hemolysis of human RBCs, respectively (Chekmenev et al., 2006). This is somewhat greater than the hemolytic activity of GAD-1 (42%) and GAD-2 (32%) with Atlantic cod RBCs at peptide concentrations of 125 μg/ml. However, amidated piscidin-3 at a concentration of 100 μg/ml exhibited 50% hemolysis while non-amidated piscidin-3 exhibited 15% hemolysis. In contrast, vespid AMPs have little hemolytic effect against rabbit RBCs at concentrations of up to 50 μg/ml (Xu et al.,

2005). In addition, hBD-3 did not exhibit (<0.5%) cytotoxic effects against human RBCs at concentrations up to 500 μg/ml (Dhople et al., 2006). Although Atlantic cod RBCs were used in the present study, AMP-induced hemolysis against mammalian RBCs may vary, and GAD-1 and GAD-2 should be tested accordingly to obtain an accurate representation of hemolytic activity in humans. These experiments will aid in determining if gaduscidins are suitable candidates for the development of novel human therapeutics.

GAD-1 and GAD-2 are paralogous transcripts (87% identity at the nucleotide level); however, they encode AMPs with a clear difference in activity and structure. It is possible that one of the gaduscidins was kept under selective evolutionary pressure due to its important function, while the other was left free to evolve another function. It is my hypothesis that GAD-1 was retained as an innate immune AMP, while GAD-2 evolved another unknown function. This is supported by our structural characterization – GAD-1 exhibited more AMP-like characteristics than GAD-2. For example, GAD-1 appeared to be more structured in the presence of deuterated SDS as determined by NMR, with a helix length of at least 13 residues compared to at least 8 residues for GAD-2. Similarly, CD spectroscopy determined that GAD-1 exhibited a clear trend toward α-helical propensity in the presence of TFE as well as zwitterionic (POPC) and anionic (POPG) liposomes. This is in contrast to GAD-2, which exhibited less structural change when exposed to the same conditions using CD and less α-helical character than GAD-1 as determined by NMR. In addition, GAD-1 also presented greater antimicrobial activity against *E. coli* and *S. intermedius* than GAD-2. It is apparent that GAD-2 may have

evolved a distinct function than GAD-1; however, more research is required to test this hypothesis.

AMPs hold much promise with respect to the development of novel antimicrobial drugs. Knowledge of AMP transcript expression, as well as physical interactions between AMPs and lipids, and antimicrobial and hemolytic activity is important in determining their mechanism of action. An important next step in the study of these AMPs is the elucidation of the exact mature peptide sequence, which should be generated by purifying these peptides from tissues where they are likely to be expressed in their mature, active form (gill for example), and subsequent sequencing. Also, anti-gaduscidin antibodies should be carried out in order to immunolocalize these peptides to particular cell types; such protein expression studies would aid in the determination of GAD-1 and GAD-2 function. In addition, gene expression studies should be carried out to ascertain the signaling pathways influencing gaduscidin expression. Furthermore, experiments whereby GAD-1 and GAD-2 are injected into a model organism (eg. mouse), and subsequent multi-tissue gene expression profiling with microarray analysis and QPCR confirmation would reveal important information. These types of microarray experiments would give an indication of which genes would be up-regulated or down-regulated if these AMPs were to be used in future clinical applications. Finally, the elucidation of GAD-1 and GAD-2 3D structures with atomic resolution are also important to determine exactly how these peptides will interact with membranous systems *in vivo*.

References

Aggarwal K, Silverman N. Positive and negative regulation of the *Drosophila* immune response. BMB Rep 2008; 41(4):267-277.

Apponyi MA, Pukala TL, Brinkworth CS, Maselli VM, Bowie JH, Tyler MJ, Booker GW, Wallace JC, Carver JA, Separovic F, Doyle J, Llewellyn LE. Host-defence peptides of Australian anurans: structure, mechanism of action and evolutionary significance. Peptides 2004; 25(6):1035-1054.

Arseniev AS, Barsukov IL, Bystrov VF, Lomize AL, Ovchinnikov Y. 1H-NMR study of gramicidin A transmembrane ion channel. Head-to-head right-handed, single-stranded helices. FEBS Lett 1985; 186(2):168-174.

Bayele HK, Srai SK. Genetic variation in hepcidin expression and its implications for phenotypic differences in iron metabolism. Haematologica 2009; 94(9):1185-1188.

Bendtsen JD, Nielsen H, von Heijne G, Brunak S. Improved prediction of signal peptides: SignalP 3.0. J Mol Biol 2004; 340(4):783-795.

Bowman S, Hubert S, Higgins B, Stone C, Kimball J, Borza T, Bussey JT, Simpson G, Kozera C, Curtis BA, Hall JR, Hori TS, Feng CY, Rise M, Booman M, Gamperl AK, Trippel E, Symonds J, Johnson SC, Rise ML. An Integrated Approach to Gene Discovery and Marker Development in Atlantic Cod (*Gadus morhua*). Mar Biotechnol in press. Accepted Apr 16, 2010.

Browne MJ, Feng CY, Booth V, Rise ML. Characterization and expression studies of Gaduscidin-1 and Gaduscidin-2; paralogous antimicrobial peptide-like transcripts from Atlantic cod (*Gadus morhua*). Dev Comp Immunol in press. Accepted Nov 16, 2010. doi:10.1016/j.dci.2010.11.010.

Campagna S, Saint N, Molle G, Aumelas A. Structure and mechanism of action of the antimicrobial peptide piscidin. Biochemistry 2007; 46(7):1771-1778.

Cellura C, Toubiana M, Parrinello N, Roch P. Specific expression of antimicrobial peptide and HSP70 genes in response to heat-shock and several bacterial challenges in mussels. Fish Shellfish Immunol 2007; 22(4):340-350.

Chekmenev EY, Vollmar BS, Forseth KT, Manion MN, Jones SM, Wagner TJ, Endicott RM, Kyriss BP, Homem LM, Pate M, He J, Raines J, Gor'kov PL, Brey WW, Mitchell DJ, Auman AJ, Ellard-Ivey MJ, Blazyk J, Cotten M. Investigating molecular recognition and biological function at interfaces using piscidins, antimicrobial peptides from fish. Biochim Biophys Acta 2006; 1758(9):1359-1372.

Chia TJ, Wu YC, Chen JY, Chi SC. Antimicrobial peptides (AMP) with antiviral activity against fish nodavirus. Fish Shellfish Immunol 2009.

Cole AM, Darouiche RO, Legarda D, Connell N, Diamond G. Characterization of a fish antimicrobial peptide: gene expression, subcellular localization, and spectrum of activity. Antimicrob Agents Chemother 2000; 44(8):2039-2045.

Cole AM, Weis P, Diamond G. Isolation and characterization of pleurocidin, an antimicrobial peptide in the skin secretions of winter flounder. J Biol Chem 1997; 272(18):12008-12013.

Conlon JM, Kolodziejek J, Nowotny N, Leprince J, Vaudry H, Coquet L, Jouenne T, King JD. Characterization of antimicrobial peptides from the skin secretions of the Malaysian frogs, *Odorrana hosii* and *Hylarana picturata* (Anura:Ranidae). Toxicon 2008; 52(3):465-473.

Davidson DJ, Currie AJ, Reid GS, Bowdish DM, MacDonald KL, Ma RC, Hancock RE, Speert DP. The cationic antimicrobial peptide LL-37 modulates dendritic cell differentiation and dendritic cell-induced T cell polarization. J Immunol 2004; 172(2):1146-1156.

Dhople V, Krukemeyer A, Ramamoorthy A. The human beta-defensin-3, an antibacterial peptide with multiple biological functions. Biochim Biophys Acta 2006; 1758(9):1499-1512.

Douglas SE, Patrzykat A, Pytyck J, Gallant JW. Identification, structure and differential expression of novel pleurocidins clustered on the genome of the winter flounder, *Pseudopleuronectes americanus* (Walbaum). Eur J Biochem 2003; 270(18):3720-3730.

Epand RM, Epand RF. Domains in bacterial membranes and the action of antimicrobial agents. Mol Biosyst 2009; 5(6):580-587.

Feng CY, Johnson SC, Hori TS, Rise M, Hall JR, Gamperl AK, Hubert S, Kimball J, Bowman S, Rise ML. Identification and analysis of differentially expressed genes in immune tissues of Atlantic cod stimulated with formalin-killed, atypical *Aeromonas salmonicida*. Physiol Genomics 2009; 37(3):149-163.

Fernandes JM, Ruangsri J, Kiron V. Atlantic cod piscidin and its diversification through positive selection. PLoS One 2010; 5(3):e9501.

Fjell CD, Hancock RE, Cherkasov A. AMPer: a database and an automated discovery tool for antimicrobial peptides. Bioinformatics 2007; 23(9):1148-1155.

Gazit E, Miller IR, Biggin PC, Sansom MS, Shai Y. Structure and orientation of the mammalian antibacterial peptide cecropin P1 within phospholipid membranes. J Mol Biol 1996; 258(5):860-870.

Goddard, TD and Kneller, DG. SPARKY 3, University of California, San Francisco.

Gul S, Smith AD, Thompson RH, Wright HP, Zilkha KJ. Fatty acid composition of phospholipids from platelets and erythrocytes in multiple sclerosis. J Neurol Neurosurg Psychiatry 1970; 33(4):506-510.

Helmerhorst EJ, Breeuwer P, van't Hof W, Walgreen-Weterings E, Oomen LC, Veerman EC, Amerongen AV, Abee T. The cellular target of histatin 5 on *Candida albicans* is the energized mitochondrion. J Biol Chem 1999; 274(11):7286-7291.

Hori TS, Gamperl AK, Afonso LO, Johnson SC, Hubert S, Kimball J, Bowman S, Rise ML. Heat-shock responsive genes identified and validated in Atlantic cod (*Gadus morhua*) liver, head kidney and skeletal muscle using genomic techniques. BMC Genomics 2010; 11:72.

Hori TS, Gamperl AK, Afonso LO, Johnson SC, Hubert S, Kimball J, Bowman S, Rise ML. Heat-shock responsive genes identified and validated in Atlantic cod (*Gadus morhua*) liver, head kidney and skeletal muscle using genomic techniques. BMC Genomics 2010; 11:72.

Hoskin DW, Ramamoorthy A. Studies on anticancer activities of antimicrobial peptides. Biochim Biophys Acta 2008; 1778(2):357-375.

Iijima N, Tanimoto N, Emoto Y, Morita Y, Uematsu K, Murakami T, Nakai T. Purification and characterization of three isoforms of chrysophsin, a novel antimicrobial peptide in the gills of the red sea bream, *Chrysophrys major*. Eur J Biochem 2003; 270(4):675-686.

Jia X, Patrzykat A, Devlin RH, Ackerman PA, Iwama GK, Hancock RE. Antimicrobial peptides protect coho salmon from *Vibrio anguillarum* infections. Appl Environ Microbiol 2000; 66(5):1928-1932.

Khandelia H, Ipsen JH, Mouritsen OG. The impact of peptides on lipid membranes. Biochim Biophys Acta 2008; 1778(7-8):1528-1536.

Kolls JK, McCray PB,Jr, Chan YR. Cytokine-mediated regulation of antimicrobial proteins. Nat Rev Immunol 2008; 8(11):829-835.

Koski LB, Gray MW, Lang BF, Burger G. AutoFACT: an automatic functional annotation and classification tool. BMC Bioinformatics 2005; 6:151.

Kragol G, Hoffmann R, Chattergoon MA, Lovas S, Cudic M, Bulet P, Condie BA, Rosengren KJ, Montaner LJ, Otvos L,Jr. Identification of crucial residues for the antibacterial activity of the proline-rich peptide, pyrrhocoricin. Eur J Biochem 2002; 269(17):4226-4237.

Lai Y, Gallo RL. AMPed up immunity: how antimicrobial peptides have multiple roles in immune defense. Trends Immunol 2009; 30(3):131-141.

Lauth X, Shike H, Burns JC, Westerman ME, Ostland VE, Carlberg JM, Van Olst JC, Nizet V, Taylor SW, Shimizu C, Bulet P. Discovery and characterization of two isoforms

of moronecidin, a novel antimicrobial peptide from hybrid striped bass. J Biol Chem 2002; 277(7):5030-5039.

Leontiadou H, Mark AE, Marrink SJ. Antimicrobial peptides in action. J Am Chem Soc 2006; 128(37):12156-12161.

Livak KJ, Schmittgen TD. Analysis of relative gene expression data using real-time quantitative PCR and the 2(-Delta Delta C(T)) Method. Methods 2001; 25(4):402-408.

Ludtke SJ, He K, Heller WT, Harroun TA, Yang L, Huang HW. Membrane pores induced by magainin. Biochemistry 1996; 35(43):13723-13728.

Luque-Ortega JR, van't Hof W, Veerman EC, Saugar JM, Rivas L. Human antimicrobial peptide histatin 5 is a cell-penetrating peptide targeting mitochondrial ATP synthesis in *Leishmania*. FASEB J 2008; 22(6):1817-1828.

Matsuzaki K, Murase O, Fujii N, Miyajima K. An antimicrobial peptide, magainin 2, induced rapid flip-flop of phospholipids coupled with pore formation and peptide translocation. Biochemistry 1996; 35(35):11361-11368.

Melo MN, Ferre R, Castanho MA. Antimicrobial peptides: linking partition, activity and high membrane-bound concentrations. Nat Rev Microbiol 2009; 7(3):245-250.

Mookherjee N, Hancock RE. Cationic host defence peptides: innate immune regulatory peptides as a novel approach for treating infections. Cell Mol Life Sci 2007; 64(7-8):922-933.

Mulero I, Noga EJ, Meseguer J, Garcia-Ayala A, Mulero V. The antimicrobial peptides piscidins are stored in the granules of professional phagocytic granulocytes of fish and are delivered to the bacteria-containing phagosome upon phagocytosis. Dev Comp Immunol 2008; 32(12):1531-1538.

Myers JK, Pace CN, Scholtz JM. Trifluoroethanol effects on helix propensity and electrostatic interactions in the helical peptide from ribonuclease T1. Protein Sci 1998; 7(2):383-388.

Nicolas P. Multifunctional host defense peptides: intracellular-targeting antimicrobial peptides. FEBS J 2009; 276(22):6483-6496.

Nielsen H, Engelbrecht J, Brunak S, von Heijne G. Identification of prokaryotic and eukaryotic signal peptides and prediction of their cleavage sites. Protein Eng 1997; 10(1):1-6.

Niyonsaba F, Someya A, Hirata M, Ogawa H, Nagaoka I. Evaluation of the effects of peptide antibiotics human beta-defensins-1/-2 and LL-37 on histamine release and prostaglandin D(2) production from mast cells. Eur J Immunol 2001; 31(4):1066-1075.

Noga EJ, Silphaduang U, Park NG, Seo JK, Stephenson J, Kozlowicz S. Piscidin 4, a Novel Member of the Piscidin Family of Antimicrobial Peptides. Comp Biochem Physiol B Biochem Mol Biol 2009.

Otvos L,Jr. Antibacterial peptides and proteins with multiple cellular targets. J Pept Sci 2005; 11(11):697-706.

Pan CY, Chen JY, Cheng YS, Chen CY, Ni IH, Sheen JF, Pan YL, Kuo CM. Gene expression and localization of the epinecidin-1 antimicrobial peptide in the grouper (*Epinephelus coioides*), and its role in protecting fish against pathogenic infection. DNA Cell Biol 2007; 26(6):403-413.

Park IY, Park CB, Kim MS, Kim SC. Parasin I, an antimicrobial peptide derived from histone H2A in the catfish, *Parasilurus asotus*. FEBS Lett 1998; 437(3):258-262.

Patrzykat A, Douglas SE. Gone gene fishing: how to catch novel marine antimicrobials. Trends Biotechnol 2003; 21(8):362-369.

Pouny Y, Rapaport D, Mor A, Nicolas P, Shai Y. Interaction of antimicrobial dermaseptin and its fluorescently labeled analogues with phospholipid membranes. Biochemistry 1992; 31(49):12416-12423.

Powers JP, Hancock RE. The relationship between peptide structure and antibacterial activity. Peptides 2003; 24(11):1681-1691.

Radyuk SN, Michalak K, Klichko VI, Benes J, Orr WC. Peroxiredoxin 5 modulates immune response in *Drosophila*. Biochim Biophys Acta 2010.

Rege K, Patel SJ, Megeed Z, Yarmush ML. Amphipathic peptide-based fusion peptides and immunoconjugates for the targeted ablation of prostate cancer cells. Cancer Res 2007; 67(13):6368-6375.

Rise ML, Hall J, Rise M, Hori T, Gamperl AK, Kimball J, Hubert S, Bowman S, Johnson SC. Functional genomic analysis of the response of Atlantic cod (*Gadus morhua*) spleen to the viral mimic polyriboinosinic polyribocytidylic acid (pIC). Dev Comp Immunol 2008; 32(8):916-931.

Rise ML, Hall JR, Rise M, Hori TS, Browne MJ, Gamperl AK, Hubert S, Kimball J, Bowman S, Johnson SC. Impact of asymptomatic nodavirus carrier state and intraperitoneal viral mimic injection on brain transcript expression in Atlantic cod (*Gadus morhua*). Physiol Genomics 2010; 42(2):266-280.

Robertson LS, Iwanowicz LR, Marranca JM. Identification of centrarchid hepcidins and evidence that 17beta-estradiol disrupts constitutive expression of hepcidin-1 and inducible expression of hepcidin-2 in largemouth bass (*Micropterus salmoides*). Fish Shellfish Immunol 2009; 26(6):898-907.

Rozek T, Wegener KL, Bowie JH, Olver IN, Carver JA, Wallace JC, Tyler MJ. The antibiotic and anticancer active aurein peptides from the Australian Bell Frogs *Litoria aurea* and *Litoria raniformis* the solution structure of aurein 1.2. Eur J Biochem 2000; 267(17):5330-5341.

Rozen S, Skaletsky H. Primer3 on the WWW for general users and for biologist programmers. Methods Mol Biol 2000; 132:365-386.

Ruangsri J, Fernandes JM, Brinchmann M, Kiron V. Antimicrobial activity in the tissues of Atlantic cod (*Gadus morhua* L.). Fish Shellfish Immunol 2010; 28(5-6):879-886.

Salerno G, Parrinello N, Roch P, Cammarata M. cDNA sequence and tissue expression of an antimicrobial peptide, dicentracin; a new component of the moronecidin family isolated from head kidney leukocytes of sea bass, *Dicentrarchus labrax*. Comp Biochem Physiol B Biochem Mol Biol 2007; 146(4):521-529.

Sass V, Pag U, Tossi A, Bierbaum G, Sahl HG. Mode of action of human beta-defensin 3 against *Staphylococcus aureus* and transcriptional analysis of responses to defensin challenge. Int J Med Microbiol 2008; 298(7-8):619-633.

Silphaduang U, Colorni A, Noga EJ. Evidence for widespread distribution of piscidin antimicrobial peptides in teleost fish. Dis Aquat Organ 2006; 72(3):241-252.

Silphaduang U, Noga EJ. Peptide antibiotics in mast cells of fish. Nature 2001; 414(6861):268-269.

Smith R, Separovic F, Milne TJ, Whittaker A, Bennett FM, Cornell BA, Makriyannis A. Structure and orientation of the pore-forming peptide, melittin, in lipid bilayers. J Mol Biol 1994; 241(3):456-466.

Song W, Shi Y, Xiao M, Lu H, Qu T, Li P, Wu G, Tian Y. In vitro bactericidal activity of recombinant human beta-defensin-3 against pathogenic bacterial strains in human tooth root canal. Int J Antimicrob Agents 2009; 33(3):237-243.

Spellberg B, Powers JH, Brass EP, Miller LG, Edwards JE,Jr. Trends in antimicrobial drug development: implications for the future. Clin Infect Dis 2004; 38(9):1279-1286.

Stark M, Liu LP, Deber CM. Cationic hydrophobic peptides with antimicrobial activity. Antimicrob Agents Chemother 2002; 46(11):3585-3590.

Strahilevitz J, Mor A, Nicolas P, Shai Y. Spectrum of antimicrobial activity and assembly of dermaseptin-b and its precursor form in phospholipid membranes. Biochemistry 1994; 33(36):10951-10960.

Subramanian S, Ross NW, MacKinnon SL. Myxinidin, a novel antimicrobial peptide from the epidermal mucus of hagfish, *Myxine glutinosa* L. Mar Biotechnol (NY) 2009; 11(6):748-757.

Sun BJ, Xie HX, Song Y, Nie P. Gene structure of an antimicrobial peptide from mandarin fish, *Siniperca chuatsi* (Basilewsky), suggests that moronecidins and pleurocidins belong in one family: the piscidins. J Fish Dis 2007; 30(6):335-343.

Tamura K, Dudley J, Nei M, Kumar S. MEGA4: Molecular Evolutionary Genetics Analysis (MEGA) software version 4.0. Mol Biol Evol 2007; 24(8):1596-1599.

Tieleman DP, Berendsen HJ, Sansom MS. An alamethicin channel in a lipid bilayer: molecular dynamics simulations. Biophys J 1999; 76(4):1757-1769.

Van Wetering S, Mannesse-Lazeroms SP, Van Sterkenburg MA, Daha MR, Dijkman JH, Hiemstra PS. Effect of defensins on interleukin-8 synthesis in airway epithelial cells. Am J Physiol 1997; 272(5 Pt 1):L888-96.

Westerhoff HV, Juretic D, Hendler RW, Zasloff M. Magainins and the disruption of membrane-linked free-energy transduction. Proc Natl Acad Sci U S A 1989; 86(17):6597-6601.

Wuthrich, K. NMR of Proteins and Nucleic Acids. 1986.

Xu X, Li J, Lu Q, Yang H, Zhang Y, Lai R. Two families of antimicrobial peptides from wasp (*Vespa magnifica*) venom. Toxicon 2006; 47(2):249-253.

Yang D, Biragyn A, Kwak LW, Oppenheim JJ. Mammalian defensins in immunity: more than just microbicidal. Trends Immunol 2002; 23(6):291-296.

Yang D, Chertov O, Oppenheim JJ. Participation of mammalian defensins and cathelicidins in anti-microbial immunity: receptors and activities of human defensins and cathelicidin (LL-37). J Leukoc Biol 2001; 69(5):691-697.

Yang, J.T. Wu C.S.C. Martinez, H.M. Calculation of protein conformation □from circular dichroism, Meth. Enzymol 1986; 130:208-269.

Yang L, Harroun TA, Weiss TM, Ding L, Huang HW. Barrel-stave model or toroidal model? A case study on melittin pores. Biophys J 2001; 81(3):1475-1485.

Zasloff M. Antimicrobial peptides of multicellular organisms. Nature 2002; 415(6870):389-395.

Zhang YM, Rock CO. Membrane lipid homeostasis in bacteria. Nat Rev Microbiol 2008; 6(3):222-233.

Zheng Y, Niyonsaba F, Ushio H, Nagaoka I, Ikeda S, Okumura K, Ogawa H. Cathelicidin LL-37 induces the generation of reactive oxygen species and release of human alpha-defensins from neutrophils. Br J Dermatol 2007; 157(6):1124-1131

Supplemental figure S1

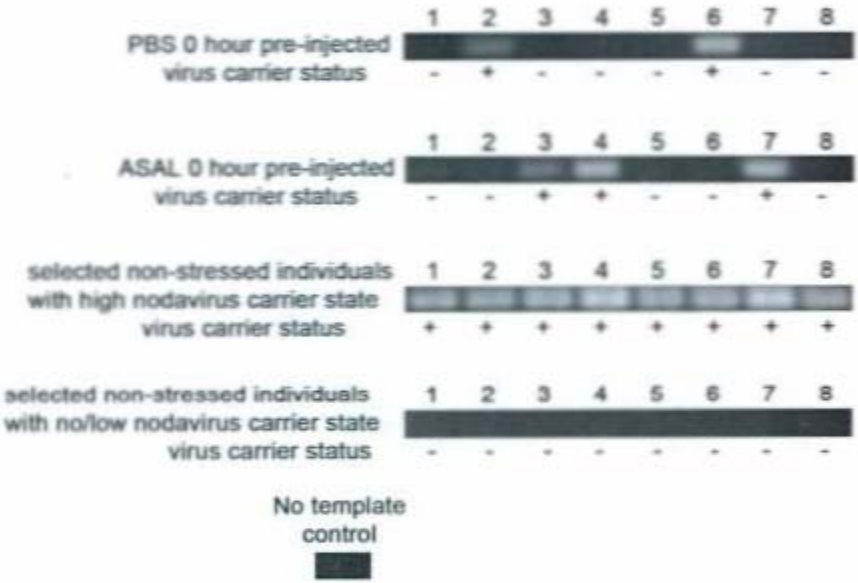

Supplemental Figure S1. Brain nodavirus RT-PCR results for fish used in the QPCR studies to determine if high nodavirus carrier state significantly influenced brain, spleen, or head kidney GAD-1 or GAD-2 transcript expression. RT-PCR was conducted on brain total RNA from 8 PBS tank 0 h (pre-injected) individuals and 8 ASAL tank 0 h (pre-injected) individuals (top 2 tiers), as well as 8 selected high nodavirus carrier state and 8 selected no/low nodavirus carrier state samples. All samples were taken from unstressed (0 h, pre-injected) fish (See footnotes of Supplemental Table S2 for details). Sample PBS 0 h fish number 4 showed a weak positive band in previous studies (Rise et al., 2008; Rise et al., 2010) that used a different RT-PCR protocol (i.e. different thermal cycler, higher quantity of cDNA template, and higher volume of PCR reaction loaded on gel); in QPCR analysis for 4 genes (ISG15, DHX58, RSAD2, and SACS), this individual behaved as a "no/low" nodavirus carrier sample (Rise et al., 2010). Sample PBS 0 h fish number 4 was categorized as a "no/low" carrier sample in the current study based on RT-PCR results. The PBS 0 h and ASAL 0 h samples were used to determine if high nodavirus carrier state significantly influenced GAD-1 or GAD-2 transcript expression (QPCR RQ values) in head kidney or spleen (Supplemental Table S5). The selected high nodavirus carrier state and no/low nodavirus carrier state samples were used to determine if high nodavirus carrier state significantly influenced GAD-1 or GAD-2 transcript expression (QPCR RQ values) in brain (Supplemental Table S4). Nodavirus RT-PCR product mean pixel intensity values for each sample can be found in Supplemental Table S2. See Materials and methods (section 2.4) for determination of carrier status designation.

Supplemental Table S1. Identification of transcripts representing GAD-1 (A) and GAD-2 (B), which were obtained from the Atlantic Cod Genomics and Broodstock Development (CGP) Expressed Sequence Tag (EST) database (http://www.codgene.ca).

A

CGP Library identifier	Library type	Tissue	Treatment	EST Accession No.
gmnlkfas	SSH forward	head kidney	ASAL	EY972641
gmnlkras	SSH reverse	head kidney	ASAL	EY974225
gmnlkras	SSH reverse	head kidney	ASAL	EY973733
gmlbgits	Normalized	gill	none	FG315806, FG315061*

B

CGP Library identifier	Library type	Tissue	Treatment	EST Accession No.
gmnbhkas	Normalized	head kidney	ASAL	ES773100, FF411786*
gmnl2pia	Normalized	blood	pIC&ASAL	FG313979
gmnlkfta	SSH forward	head kidney	heat shock	EX190088
gmnlsfic	SSH forward	spleen	pIC	ES784714
gmnlsfic	SSH forward	spleen	pIC	ES786084
gmnlsfic	SSH forward	spleen	pIC	ES785365
gmnlsfic	SSH forward	spleen	pIC	ES787243

*ESTs that were generated from the same clone were listed in the same row.

Supplemental Table S2. Mean pixel intensities of nodavirus RT-PCR products from individual Atlantic cod brain samples involved in this study.

ASAL and PBS sample ID[1]	Mean pixel intensity	Carrier status	Brain study sample ID[2]	Mean pixel intensity	Carrier status
ASAL 0h 1	4465	no/low	1	24212	high
ASAL 0h 2	3831	no/low	2	25182	high
ASAL 0h 3	12240	high	3	28135	high
ASAL 0h 4	21964	high	4	33733	high
ASAL 0h 5	3706	no/low	5	26939	high
ASAL 0h 6	3143	no/low	6	29076	high
ASAL 0h 7	21466	high	7	33658	high
ASAL 0h 8	957	no/low	8	25615	high
PBS 0h 1	662	no/low	9	5887	no/low
PBS 0h 2	10973	high	10	5198	no/low
PBS 0h 3	1323	no/low	11	4618	no/low
PBS 0h 4	1959	no/low	12	4224	no/low
PBS 0h 5	2664	no/low	13	3735	no/low
PBS 0h 6	22980	high	14	3175	no/low
PBS 0h 7	3538	no/low	15	2179	no/low
PBS 0h 8	2995	no/low	16	1073	no/low

[1]The sample ID correspond the the sampe ID referred in Supplemental Table S5 and S6.
[2]Sample 1, 2, 9, and 10 are individuals from the 0 h undisturbed control group in Rise et al., 2008.
[2]Sample 3 and 4 are technical replicates of PBS 0h 2 and PBS 0h 6, respectively.
[2]Sample 5 and 6 are technical replicates of ASAL 0h 3 and ASAL 0h 4, respectively.
[2]Sample 11 and 12 are technical replicates of PBS 0h 1 and PBS 0h 3, respectively.
[2]Sample 13 and 14 are technical replicates of ASAL 0h 6 and ASAL 0h 8, respectively.
[2]Sample 7, 8, 15, and 16 are individuals from the 0 h pre-injected polyriboinosinic polyribocytidylic acid group in Rise et al., 2008.

Supplemental Table S3. QPCR Relative Quantification (RQ) Data for the constitutive expression study of GAD-1 (A) and GAD-2 (B), normalized to 18S Ribosomal RNA.

A

Tissue	No[1]	RQ	Ave.RQ	SD	SEM
Blood	2	10.61	25.81	17.59	8.79
Blood	5	30.30			
Blood	6	13.55			
Blood	7	48.76			
Brain	2	1.48	2.58	1.65	0.67
Brain	3	3.54			
Brain	4	3.18			
Brain	5	1			
Brain	6	1.13			
Brain	7	5.13			
Gill	2	9.15	201.84	321.39	131.12
Gill	3	368.79			
Gill	4	789.53			
Gill	5	22.45			
Gill	6	4.51			
Gill	7	16.63			
Head kidney	2	59.96	322.23	326.32	133.22
Head kidney	3	749.35			
Head kidney	4	712.77			
Head kidney	5	81.00			
Head kidney	6	62.31			
Head kidney	7	267.97			
Pyloric caecum	2	7.971	10.85	11.17	4.56
Pyloric caecum	3	11.87			
Pyloric caecum	4	32.68			
Pyloric caecum	5	2.31			
Pyloric caecum	6	5.01			
Pyloric caecum	7	5.25			
Spleen	2	461.81	406.10	360.64	147.23
Spleen	3	597.3			
Spleen	4	1011.12			
Spleen	5	90.75			
Spleen	6	114.10			
Spleen	7	161.44			

B

Tissue	No	RQ	Ave.RQ	SD	SEM
Blood	2	292.72	442.93	365.17	182.59
Blood	5	385.87			
Blood	6	126.60			
Blood	7	966.34			
Brain	2	1	2.99	1.89	0.77
Brain	3	4.20			
Brain	4	1.78			
Brain	5	3.49			
Brain	6	1.52			
Brain	7	5.93			
Gill	2	837.64	605.31	348.23	142.16
Gill	3	432.96			
Gill	4	1187.16			
Gill	5	588.86			
Gill	6	233.79			
Gill	7	371.45			
Head kidney	2	594.66	635.72	329.42	134.49
Head kidney	3	392.38			
Head kidney	4	1294.93			
Head kidney	5	504.26			
Head kidney	6	502.99			
Head kidney	7	525.88			
Pyloric caecum	2	3.50	5.77	4.36	1.78
Pyloric caecum	3	2.30			
Pyloric caecum	4	13.29			
Pyloric caecum	5	4.29			
Pyloric caecum	6	2.51			
Pyloric caecum	7	8.71			
Spleen	2	1311.24	1843.86	1581.47	645.63
Spleen	3	671.16			
Spleen	4	4162.26			
Spleen	5	448.48			
Spleen	6	966.48			
Spleen	7	3503.52			

[1]The individual 1 was not selected due to compromised template quality.
For blood, the normalizer CT values of individuals 3 and 4 were outliers,
and these two individuals were removed from the analysis.

Supplemental Table S4. QPCR Relative Quantification (RQ) data for GAD-1 (A) and GAD-2 (B) and analysis of any impact of nodavirus carrier status on these genes in the brain, normalized to 18S Ribosomal RNA.

A

Sample ID[1]	Carrier status	Mean pixel intensity	RQ	Ave. RQ	SD	SEM
1	high	24212	10.75	8.29	5.98	2.11
2	high	25182	19.65			
3	high	28135	11.20			
4	high	33733	3.15			
5	high	26939	4.73			
6	high	29076	3.34			
7	high	33658	11.14			
8	high	25615	2.37			
9	no/low	5887	2.23	4.69	3.14	1.11
10	no/low	5198	4.52			
11	no/low	4618	1.00			
12	no/low	4224	9.93			
13	no/low	3735	1.44			
14	no/low	3175	7.80			
15	no/low	2179	5.98			
16	no/low	1073	4.63			

[1]The sample ID correspond the sample ID referred in Supplemental Table S2, see footnotes of Supplemental Table S2 for more details.

B

Sample ID	Carrier status	Mean pixel intensity	RQ	Ave. RQ	SD	SEM
1	high	24212	7.39	4.70	2.44	0.86
2	high	25182	8.93			
3	high	28135	5.00			
4	high	33733	4.11			
5	high	26939	3.16			
6	high	29076	1.40			
7	high	33658	4.64			
8	high	25615	2.99			
9	no/low	5887	7.08	5.11	3.33	1.18
10	no/low	5198	3.16			
11	no/low	4618	4.74			
12	no/low	4224	3.57			
13	no/low	3735	1.00			
14	no/low	3175	4.15			
15	no/low	2179	5.01			
16	no/low	1073	12.14			

Supplemental Table S5. QPCR Relative Quantification (RQ) data for the study determining any effect of nodavirus status on non-stressed (0 h) immune tissues, normalized to 18S Ribosomal RNA

Supplemental Table S5A. QPCR analysis of GAD-1 expression in non-stressed (0 h) cod head kidney tissue and determination of any impact of nodavirus-carrier status on its expression

Treatment tank	Time point	No[1]	Mean pixel intensity	Carrier status	RQ	Ave. RQ	SD	SEM
PBS	0	1	662	no/low	4.33	10.84	7.71	3.15
PBS	0	2	10973	high	17.60			
PBS	0	3	1323	no/low	22.55			
PBS	0	4	1959	no/low	3.15			
PBS	0	5	2664	no/low	10.11			
PBS	0	6	22980	high	7.32			
Asal	0	3	12240	high	18.35	7.49	7.35	3.29
Asal	0	4	21964	high	11.85			
Asal	0	5	3706	no/low	2.29			
Asal	0	6	3143	no/low	1.39			
Asal	0	7	21466	high	3.60			

[1]As obtained from Supplemental Table S2.

Supplemental Table S5B. QPCR analysis of GAD-2 expression in non-stressed (0 h) cod head kidney tissue and determination of any impact of nodavirus-carrier status on its expression

Treatment tank	Time point	No	Mean pixel intensity	Carrier status	RQ	Ave. RQ	SD	SEM
PBS	0	1	662	no/low	12.63	10.16	1.89	0.77
PBS	0	2	10973	high	11.43			
PBS	0	3	1323	no/low	9.77			
PBS	0	4	1959	no/low	8.12			
PBS	0	5	2664	no/low	7.93			
PBS	0	6	22980	high	11.09			
Asal	0	3	12240	high	4.55	5.09	1.63	0.73
Asal	0	4	21964	high	7.37			
Asal	0	5	3706	no/low	4.44			
Asal	0	6	3143	no/low	3.10			
Asal	0	7	21466	high	6.00			

Supplemental Table S5C. QPCR analysis of GAD-1 expression in non-stressed (0 h) cod spleen tissue and determination of any impact of nodavirus-carrier status on its expression

Treatment tank	Time point	No	Mean pixel intensity	Carrier status	RQ	Ave. RQ	SD	SEM
PBS	0	1	662	no/low	5.96	7.76	5.86	2.39
PBS	0	2	10973	high	7.23			
PBS	0	3	1323	no/low	16.68			
PBS	0	4	1959	no/low	1.55			
PBS	0	5	2664	no/low	12.57			
PBS	0	6	22980	high	2.57			
Asal	0	2	3831	no/low	4.60	6.97	7.03	2.87
Asal	0	3	12240	high	18.82			
Asal	0	4	21964	high	12.26			
Asal	0	5	3706	no/low	1.34			
Asal	0	6	3143	no/low	2.53			
Asal	0	7	21466	high	2.29			

Supplemental Table S5D. QPCR analysis of GAD-2 expression in non-stressed (0 h) cod spleen tissue and determination of any impact of nodavirus-carrier status on its expression

Treatment tank	Time point	No	Mean pixel intensity	Carrier status	RQ	Ave. RQ	SD	SEM
PBS	0	1	662	no/low	3.29	3.68	1.06	0.43
PBS	0	2	10973	high	3.87			
PBS	0	3	1323	no/low	4.74			
PBS	0	4	1959	no/low	3.48			
PBS	0	5	2664	no/low	4.77			
PBS	0	6	22980	high	1.91			
Asal	0	2	3831	no/low	9.16	5.83	3.07	1.25
Asal	0	3	12240	high	2.91			
Asal	0	4	21964	high	9.26			
Asal	0	5	3706	no/low	3.98			
Asal	0	6	3143	no/low	2.57			
Asal	0	7	21466	high	7.10			

Supplemental Table S6. QPCR Relative Quantification (RQ) data for the immune tissue (head kidney and spleen) study, normalized to 18S ribosomal RNA.

Supplemental Table S6A. QPCR analysis of GAD-1 expression in head kidney

Treatment tank	Time point	No[1]	RQ	Ave. RQ	SD	SEM	Fold up-regulated (Ave. RQ)/(Ave. 0hr RQ)	Fold down-regulated 1/(fold up-regulated)
PBS	0	1	4.33	10.84	7.71	3.15	1.0	1.0
PBS	0	2	17.60					
PBS	0	3	22.55					
PBS	0	4	3.15					
PBS	0	5	10.11					
PBS	0	6	7.32					
PBS	2	1	13.14	5.79	5.76	2.18	0.5	1.9
PBS	2	2	1.45					
PBS	2	3	1.70					
PBS	2	4	2.33					
PBS	2	5	6.08					
PBS	2	6	14.55					
PBS	2	7	1.25					
PBS	6	1	5.91	3.85	3.30	1.25	0.4	2.8
PBS	6	2	3.47					
PBS	6	3	10.35					
PBS	6	4	1.80					
PBS	6	5	1.51					
PBS	6	6	1.00					
PBS	6	7	2.92					
PBS	24	1	6.12	10.07	5.92	2.24	0.9	1.1
PBS	24	2	10.27					
PBS	24	3	8.11					
PBS	24	4	3.47					
PBS	24	5	12.37					
PBS	24	6	8.32					
PBS	24	7	21.86					
PBS	72	3	11.05	14.00	2.21	0.99	1.3	0.8
PBS	72	4	15.88					
PBS	72	5	16.50					
PBS	72	6	13.36					
PBS	72	7	13.23					
Asal	0	3	18.35	7.49	7.35	3.29	1.0	1.0
Asal	0	4	11.85					
Asal	0	5	2.29					
Asal	0	6	1.39					
Asal	0	7	3.60					

Asal	2	1	3.42	8.13	7.70	2.91	1.1	0.9
Asal	2	2	2.33					
Asal	2	3	2.06					
Asal	2	4	14.55					
Asal	2	5	21.58					
Asal	2	6	10.68					
Asal	2	7	2.29					
Asal	6	1	1.92	9.11	6.14	2.51	1.2	0.8
Asal	6	2	4.17					
Asal	6	3	6.99					
Asal	6	4	17.43					
Asal	6	5	8.84					
Asal	6	6	15.31					
Asal	24	1	1.88	3.28	3.13	1.18	0.4	2.3
Asal	24	2	1.00					
Asal	24	3	1.06					
Asal	24	4	1.22					
Asal	24	5	4.56					
Asal	24	6	3.59					
Asal	24	7	9.65					
Asal	72	1	6.29	6.83	1.33	0.50	0.9	1.1
Asal	72	2	8.17					
Asal	72	3	8.41					
Asal	72	4	7.51					
Asal	72	5	6.91					
Asal	72	6	5.71					
Asal	72	7	4.77					

[1]The individual ASAL 0H 1 was not selected due to compromised template quality. Also, the normalizer CT values of PBS 0H individual 7, PBS 72H individuals 1 and 2, ASAL 0H individual 2 and ASAL 6H individual 7 were outliers, and these individuals were removed from the analysis.

Supplemental Table S6B. QPCR analysis of GAD-2 expression in head kidney

Treatment tank	Time point	No[1]	RQ	Ave. RQ	SD	SEM	Fold up-regulated (Ave. RQ)/(Ave. 0hr RQ)	Fold down-regulated 1/(fold up-regulated)
PBS	0	1	12.63	10.16	1.89	0.77	1.0	1.0
PBS	0	2	11.43					
PBS	0	3	9.77					
PBS	0	4	8.12					
PBS	0	5	7.93					
PBS	0	6	11.09					
PBS	2	1	9.85	9.74	3.93	1.48	1.0	1.0
PBS	2	2	11.83					
PBS	2	3	10.64					
PBS	2	4	11.64					
PBS	2	5	11.29					
PBS	2	6	11.94					
PBS	2	7	1.00					
PBS	6	1	7.72	8.64	4.11	1.55	0.9	1.2
PBS	6	2	5.44					
PBS	6	3	7.36					
PBS	6	4	16.23					
PBS	6	5	6.42					
PBS	6	6	12.25					
PBS	6	7	5.05					
PBS	24	1	8.39	10.08	5.65	2.14	1.0	1.0
PBS	24	2	19.80					
PBS	24	3	6.51					
PBS	24	4	11.09					
PBS	24	5	8.04					
PBS	24	6	2.43					
PBS	24	7	14.28					
PBS	72	3	14.96	10.72	3.76	1.68	1.1	0.9
PBS	72	4	6.74					
PBS	72	5	8.40					
PBS	72	6	14.50					
PBS	72	7	9.00					
Asal	0	3	4.55	5.09	1.63	0.73	1.0	1.0
Asal	0	4	7.37					
Asal	0	5	4.44					
Asal	0	6	3.10					
Asal	0	7	6.00					
Asal	2	1	4.86	4.07	2.89	1.09	0.8	1.2
Asal	2	2	3.62					
Asal	2	3	1.19					
Asal	2	4	2.49					
Asal	2	5	5.21					

Asal	2	6	1.54					
Asal	2	7	9.61					
Asal	6	1	2.60	3.63	1.32	0.54	0.7	1.4
Asal	6	2	2.57					
Asal	6	3	3.12					
Asal	6	4	3.28					
Asal	6	5	4.15					
Asal	6	6	6.07					
Asal	24	1	3.52	5.08	2.87	1.08	1.0	1.0
Asal	24	2	3.02					
Asal	24	3	3.89					
Asal	24	4	9.38					
Asal	24	5	1.36					
Asal	24	6	7.16					
Asal	24	7	7.23					
Asal	72	1	1.69	1.87	0.81	0.31	0.4	2.7
Asal	72	2	2.98					
Asal	72	3	2.73					
Asal	72	4	1.00					
Asal	72	5	2.31					
Asal	72	6	1.02					
Asal	72	7	1.34					

[1]The individual ASAL 0H 1 was not selected due to compromised template quality. Also, the normalizer CT values of PBS 0H individual 7, PBS 72H individuals 1 and 2, ASAL 0H individual 2 and ASAL 6H individual 7 were outliers, and these individuals were removed from the analysis.

Supplemental Table S6C. QPCR analysis of GAD-1 expression in spleen

Treatment tank	Time point	No[1]	RQ	Ave. RQ	SD	SEM	Fold up-regulated (Ave. RQ)/(Ave. 0hr RQ)	Fold down-regulated 1/(fold up-regulated)
PBS	0	1	5.96	7.76	5.86	2.39	1.0	1.0
PBS	0	2	7.23					
PBS	0	3	16.68					
PBS	0	4	1.55					
PBS	0	5	12.57					
PBS	0	6	2.57					
PBS	2	1	29.80	13.96	11.32	4.62	1.8	0.6
PBS	2	2	3.73					
PBS	2	3	4.27					
PBS	2	4	12.19					
PBS	2	5	7.61					
PBS	2	6	26.13					
PBS	6	4	1.79	1.37	0.40	0.23	0.2	5.7
PBS	6	5	1.32					
PBS	6	6	1.00					
PBS	24	3	16.07	10.85	5.14	2.30	1.4	0.7
PBS	24	4	3.31					
PBS	24	5	13.70					
PBS	24	6	13.15					
PBS	24	7	8.02					
PBS	72	2	3.37	8.43	6.69	3.35	1.1	0.9
PBS	72	3	4.18					
PBS	72	4	17.95					
PBS	72	5	8.22					
Asal	0	2	4.60	6.97	7.03	2.87	1.0	1.0
Asal	0	3	18.82					
Asal	0	4	12.26					
Asal	0	5	1.34					
Asal	0	6	2.53					
Asal	0	7	2.29					
Asal	2	2	3.37	24.78	21.93	9.81	3.6	0.3
Asal	2	3	8.52					
Asal	2	4	36.76					
Asal	2	5	18.54					
Asal	2	6	56.70					
Asal	6	2	14.40	11.69	3.86	1.73	1.7	0.6
Asal	6	3	12.88					
Asal	6	4	10.00					
Asal	6	5	15.35					

Asal	6	6	5.82					
Asal	24	2	1.77	4.74	5.76	2.35	0.7	1.5
Asal	24	3	1.00					
Asal	24	4	1.13					
Asal	24	5	3.71					
Asal	24	6	4.72					
Asal	24	7	16.10					
Asal	72	1	8.18	8.77	3.74	1.41	1.3	0.8
Asal	72	2	10.15					
Asal	72	3	3.75					
Asal	72	4	7.99					
Asal	72	5	5.39					
Asal	72	6	10.84					
Asal	72	7	15.11					

[1]The individuals PBS 6H 1, 2 and 3, as well as ASAL 0H 1 were not selected due to compromised template quality. Also, the normalizer CT values of PBS 0H individual 7, PBS 2H individual 7, PBS 6H individual 7, PBS 24H individuals 1 and 2, PBS 72H individuals 1,6 and 7, ASAL 2H individuals 1 and 7, ASAL 6H individuals 1 and 7, and ASAL 24H individual 1 were outliers, and these individuals were removed from the analysis.

Supplemental Table S6D. QPCR analysis of GAD-2 expression in spleen

Treatment tank	Time point	No[1]	RQ	Ave. RQ	SD	SEM	Fold up-regulated (Ave. RQ)/(Ave. 0hr RQ)	Fold down-regulated 1/(fold up-regulated)
PBS	0	1	3.29	3.68	1.06	0.43	1.0	1.0
PBS	0	2	3.87					
PBS	0	3	4.74					
PBS	0	4	3.48					
PBS	0	5	4.77					
PBS	0	6	1.91					
PBS	2	1	9.86	7.89	2.11	0.86	2.1	0.5
PBS	2	2	9.89					
PBS	2	3	6.10					
PBS	2	4	9.35					
PBS	2	5	4.97					
PBS	2	6	7.20					
PBS	6	4	7.01	5.30	1.84	1.06	1.4	0.7
PBS	6	5	5.52					
PBS	6	6	3.36					
PBS	24	3	5.48	4.14	2.27	1.01	1.1	0.9
PBS	24	4	6.92					
PBS	24	5	4.43					
PBS	24	6	2.64					
PBS	24	7	1.20					
PBS	72	2	1.00	3.50	1.74	0.87	1.0	1.1
PBS	72	3	4.13					
PBS	72	4	5.03					
PBS	72	5	3.83					
Asal	0	2	9.16	5.83	3.07	1.25	1.0	1.0
Asal	0	3	2.91					
Asal	0	4	9.26					
Asal	0	5	3.98					
Asal	0	6	2.57					
Asal	0	7	7.10					
Asal	2	2	7.69	8.35	4.85	2.17	1.4	0.7
Asal	2	3	5.27					
Asal	2	4	11.71					
Asal	2	5	2.51					
Asal	2	6	14.58					
Asal	6	2	13.29	12.29	6.75	3.02	2.1	0.5
Asal	6	3	6.98					
Asal	6	4	14.35					
Asal	6	5	21.98					

Asal	6	6	4.86					
Asal	24	2	6.32	7.21	4.39	1.79	1.2	0.8
Asal	24	3	4.42					
Asal	24	4	12.86					
Asal	24	5	1.03					
Asal	24	6	11.43					
Asal	24	7	7.23					
Asal	72	1	2.65	3.55	2.00	0.76	0.6	1.6
Asal	72	2	7.45					
Asal	72	3	3.77					
Asal	72	4	1.00					
Asal	72	5	3.88					
Asal	72	6	2.39					
Asal	72	7	3.70					

[1]The individuals PBS 6H 1, 2 and 3, as well as ASAL 0H 1 were not selected due to compromised template quality. Also, the normalizer CT values of PBS 0H individual 7, PBS 2H individual 7, PBS 6H individual 7, PBS 24H individuals 1 and 2, PBS 72H individuals 1,6 and 7, ASAL 2H individuals 1 and 7, ASAL 6H individuals 1 and 7, and ASAL 24H individual 1 were outliers, and these individuals were removed from the analysis.